

RHIC Beam Use Request For Runs 12 and 13

The STAR Collaboration
May 16, 2011

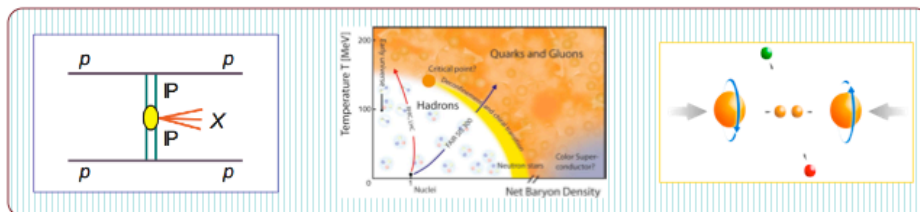
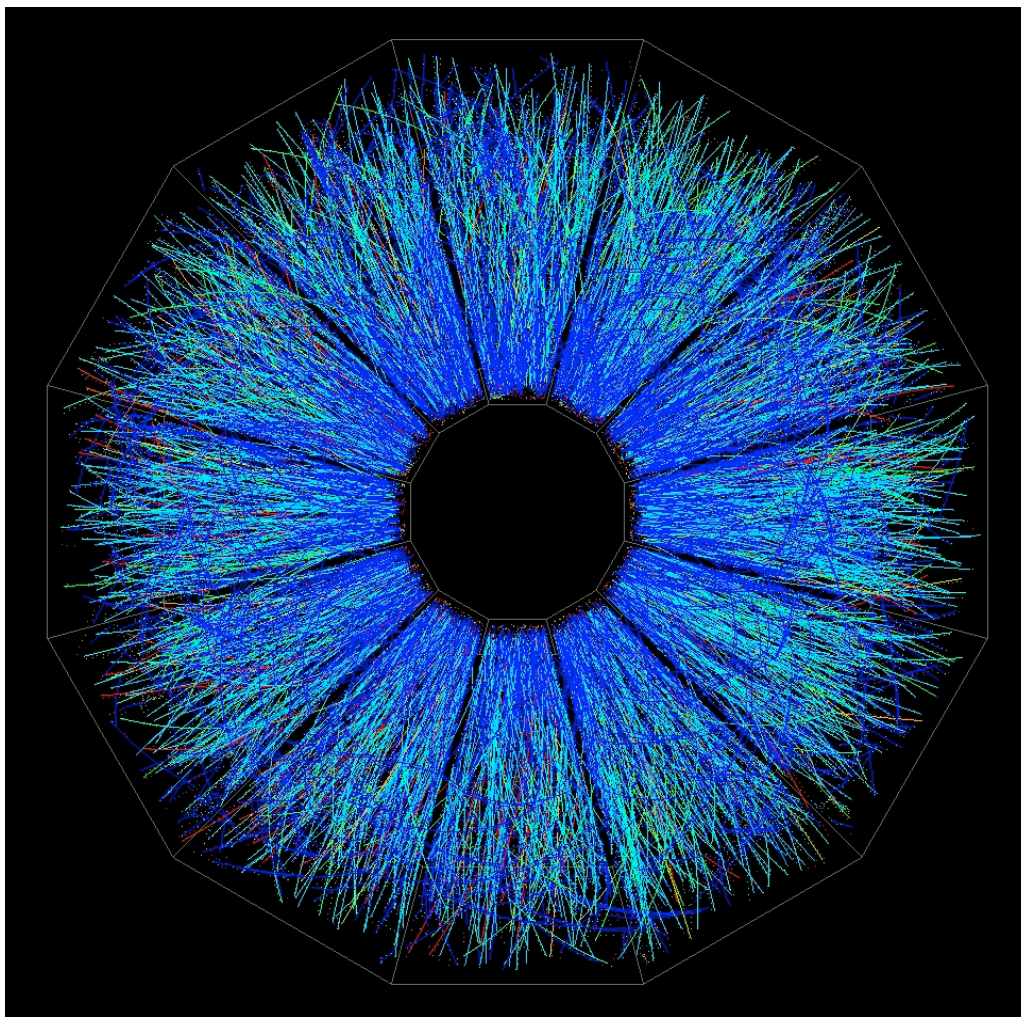


Table of Contents

1. Executive Summary	3
2. Report on Run 11 Performance and Progress on Data Analysis.....	6
2.1 Introduction.....	6
2.2 Run 11 Detector Performance and Statistics.....	6
3. Study of the QCD Phase Diagram and the Properties of QGP.....	8
3.1 Completion of Phase-I of Beam Energy Scan Program in Run 12	8
3.2 Physics Results to Date from Phase-I of Beam Energy Scan	9
3.3 Summary of Noteworthy Preliminary Result from the Beam Energy Scan	16
3.4 Physics of 200 GeV U+U Collisions at RHIC	17
4. Study of p+p Collisions	25
4.1 Introduction	25
4.2 Recent Results from 200 GeV p+p Collisions during Run 9	26
4.3 Performance and Experience from Run 11	27
4.4 Request for Run 12	29
4.4.1 Forward GEM Track (FGT) Commissioning and W-physics Measurements ...	29
4.4.2 The pp2pp Measurements	34
4.5 Scenarios for Run 13	35
4.5.1 Polarized p+p Collisions in Run 13	35
4.5.2 Heavy Ion Reference p+p Collisions in Run 13	38
5. STAR Heavy Flavor Tracker (HFT) Engineering Run	41

RHIC Beam Use Request
For Runs 12 and 13

The STAR Collaboration

May 16, 2011

1. Executive Summary

The STAR Collaboration makes the following two-year beam-use proposal, in order to achieve its spin and relativistic heavy ion physics goals on a timescale consistent with intense international interest and competition in these areas, as well as to utilize RHIC beams effectively, taking full advantage of planned improvements in machine and detector capability as a function of time:

Run	Energy	Time	System	Goal
12 ⁽¹⁾	$\sqrt{s_{NN}} = 27$ GeV	1 week	Au + Au	150M minbias
	$\sqrt{s} = 500$ GeV	3 weeks	p- p-	FGT commissioning $P^{2*} \mathcal{L} = 42$ pb ⁻¹ $P^{4*} \mathcal{L} = 12$ pb ⁻¹
		9 weeks		
	$\sqrt{s_{NN}} = 193$ GeV	1 week	pp2pp	pp2pp at high β^*
6 weeks		U + U	200M minbias 200M central	
13 ⁽²⁾	$\sqrt{s} = 500$ GeV	8 weeks	p- p-	$P^{2*} \mathcal{L} = 50$ pb ⁻¹
	$\sqrt{s} = 200$ GeV	10 weeks	p, p _r	$P^{2*} \mathcal{L} = 7.2$ pb ⁻¹ $P^{4*} \mathcal{L} = 7.1$ pb ⁻¹ $\mathcal{L} = 60$ pb ⁻¹
			p- p-	
$\sqrt{s_{NN}} = 200$ GeV	6 weeks	Au+Au	HFT & MTD engineering run	

Table 1.1: STAR Beam Use Request for Runs 12 and 13.

(1) 26 cryo weeks, 6 weeks for overhead and initial commissioning of three species. Total of 20 weeks production with three species

(2) 30 cryo weeks, 24 weeks production with two species.

In this proposed physics-driven plan, the STAR Collaboration intends to make the most efficient use of RHIC beam time and upgrades in order to make timely progress in determining the QCD phase structure within the reach of RHIC, the properties of the new state of matter produced at top RHIC energy, to map the x dependence of the gluon polarization in the proton, $\Delta g(x)$, and to delineate the polarizations of the light quark and anti-quarks in the proton, $\Delta q(x)$, by flavor.

The primary goals of the proposed program are:

Run 12: 26 cryo-weeks, 20 weeks for physics production with three species:

- a) One week: $\sqrt{s_{NN}} = 27$ GeV Au+Au collisions. Search for the existence and location of the QCD critical point. Complete the Phase-I Beam energy Scan (BES) program at RHIC. Note that the 27 GeV Au+Au collisions will be used for part of the FGT commissioning during the Run.
- b) Three weeks: 500 GeV pp collisions for FGT commissioning. We anticipate that at least 12 FGT quadrants (out of 24) will be ready for Run 12. These data will also contribute to the measurements of A_L for W production at $-1 < \eta < 1$ and $\Delta g(x)$.
- c) Nine weeks: 500 GeV p+p collisions to collect $FOM = 42 \text{ pb}^{-1}$ W physics data at both mid- and forward- rapidity and $FOM = 12 \text{ pb}^{-1}$ for gluon polarization, $\Delta g(x)$. A 50% or better polarization of the proton beams has been assumed in our estimation. This will be the initial physics production run after first installation of the Forward GEM Tracker (FGT) for the measurement of the parity violating single spin asymmetry, A_L , in W production at forward-rapidity. This program requires longitudinally polarized p+p collisions at $\sqrt{s} = 500$ GeV and aims, in several years of running, to sample a total of 300 pb^{-1} with 70% beam polarization.
- d) One week: 500 GeV collisions with high $\beta^* = 7.5\text{m}$. Continue the pp2pp program with Roman Pots begun in Run 9, with transversely polarized beams, for studies of diffractive physics including spin dependence and coincident central particle production. This will yield the first data at $\sqrt{s} = 500$ GeV with the Roman Pots.
- e) Six weeks: $\sqrt{s_{NN}} = 193$ GeV U+U collisions in order to study in more detail the properties of matter produced at top RHIC energy.

Run 13: 30 cryo-weeks, 24 weeks for physics production with two species:

- a) Eight weeks: 500 GeV longitudinally polarized p+p collision for W-physics measurements.
- b) Ten weeks: 200 GeV polarized p+p collisions. Note that for transverse single spin asymmetry measurement, a polarization of 60% or better is assumed and for the longitudinally doubly asymmetry measurements, a polarization of 65% or better is required. The integrated 60pb^{-1} luminosity of the p+p collisions will also be used as reference data for heavy ion physics analysis.

- c) Six weeks: $\sqrt{s_{\text{NN}}} = 200$ GeV Au+Au collisions for both the Heavy Flavor Tracker (HFT) and Muon Telescope Detector (MTD) engineering.

2. Report on Run 11 Performance

2.1 Introduction

Three measurements have been made during the Run11 period: (i) 500 GeV transverse polarized p+p collisions with the STAR FMS detector; (ii) $\sqrt{s_{NN}} = 19.6$ GeV Au+Au collisions as part of the Phase-I Beam Energy Scan Program at RHIC. The goal here is to search for the existence and the location of the QCD phase boundary and the possible critical point; (iii) $\sqrt{s_{NN}} = 200$ GeV Au+Au collisions for six weeks.

2.2 Run 11 Detector Performance and Statistics

In Run 10, the STAR detectors were positioned to take data for top energy Au+Au collisions and the Phase-I BES program at different energies. Table 1 shows the changes/upgrades to the detectors and their electronics. The new additions are the fully complete Time-of-Flight Detector, a new Trigger-Clock Unit (TCU), online tracking on every event by a high-level trigger (HLT), and rework of the readout electronics of the Barrel EMC Shower-Maximum Detector.

Component	TOF Time-of-Flight Detector (% installed)	FTPC+PMD Forward TPC Photon- Multiplicity Detector	TCU Trigger- Clock Unit	BSMD Barrel EMC Shower- Max Electronics	FMS Forward Meson Spectro- meter	HLT High- Level Trigger
Physics	Dilepton, PID correlation and fluctuation	Reaction Plane, Flow, DCC	General	Jet, Heavy- flavor	CGC, Trans. Spin	High-p _T , J/Ψ, Exotic
Run 9 p+p	75%	OFF	16bits	15% dead-time @300Hz	ON	TEST
Run 10 200 BES	100%	ON Repairs of PMD electronics	128bits	15% dead-time @600Hz	OFF	Online tracking on, every event
Run 11 500 GeV p+p Au+Au	100%	OFF	128bits		ON	ON

Table 2.1: *Detector configuration in Run 9, Run 10 and Run 11.*

A High-Level trigger was deployed this run with online tracking on every triggered event from Level 0. The 24 Sector Level 3 (SL3) machines, which are used for the TPC data acquisition and cluster finding, are also used in sector-by-sector tracking. Tracks, tower

information from the BEMC detector, time of flight from the TOF detector are sent to Global Level 3 (GL3) machines, in which the complete event is reconstructed and a trigger decision is made. During Run 11, after the goals for minimum-bias and central collision events were reached, the HLT acted as a trigger decision in selecting interesting events to record.

During the 500 GeV p+p run, the averaged polarization (transverse) for both rings are around 48% and STAR collected 27pb^{-1} FMS high p_T trigger data ($\sim 110\text{M}$ mini bias events). The collected statistics is more than STAR originally requested. For the $\sqrt{s_{NN}} = 19.6$ GeV Au+Au collisions, STAR collected about 85M mini bias events and 17M of them are good events in terms of the quality. Since May 5th, we started the $\sqrt{s_{NN}} = 200$ GeV Au+Au run. This year, the detector materials between the beam pipe and TPC inner field cage are minimized. We plan to collect 700 - 800 M mini bias events for the full azimuthal coverage dielectron analysis. The EMC high tower trigger will enrich the data with heavy flavor Upsilon production in heavy ion collisions.

3. Study of the QCD Phase Diagram and Properties of QGP

3.1 Completion of Phase-I of Beam Energy Scan Program in Run 12

The Critical Point (CP) search part of the BES program requires a careful choice of stepping in μ_B for this experimentally-driven approach to locate a possible CP. A non-monotonic dependence of observables sensitive to CP on $\sqrt{s_{NN}}$ and an increase of long-wavelength fluctuations should become apparent only near the critical point. The rise and then fall of this signal as μ_B increases should allow us to ascertain the (T, μ_B) coordinates of the critical point. Note that the magnitude of these non-monotonic excursions, as well as the probability that they will survive the final state interactions, is difficult to predict. Fortunately for the experiments, there may not be a need for the evolution trajectory of the system to “pass” precisely through the critical point in the (T, μ_B) plane to see the signatures, as some hydrodynamic calculations show that the critical point “attracts” trajectories [1]. In such a case, if the trajectory misses the critical point by a few tens of MeV along the μ_B axis, the signature will be just as strong as if it were to pass directly through it. Note, however, that this “attraction” is not generic, and relies on specific features of the EOS near the critical point [1]. Available lattice QCD calculations suggest the μ_B region of influence around CP would be around 100 MeV [2].

Although subsequent phases of BES running will use smaller steps in μ_B to verify and trace the possible effect of focusing and to pin down the critical point, the first exploration phase was proposed to step in μ_B such that with a few steps in $\sqrt{s_{NN}}$, we may narrow down to an area of interest for further study (see Table 3.1 for the beam energies and corresponding μ_B values [3]). Thus 19.6 and 27 GeV collisions crucially bridge the gap in μ_B corresponding to about 200 MeV between 39 and 11.5 GeV collisions for which STAR took data in Run 10.

Beam Energy (GeV)	Baryon Chemical Potential, μ_B (MeV)
5.0	550
7.7	410
11.5	300
19.6	230
27	151
39	112

Table 3.1: *Beam energies and corresponding expected baryon chemical potentials.*

The following is our proposal for completion of Phase-I of the BES program in Run 12. It is consistent with the BUR for Runs 10 – 11 and with the PAC recommendation, but has been updated to reflect information from data-taking to date. Both event rates and data taking efficiency were higher than expected before Run 10, with an average of approximately 85 hours/week of data taking at energies above injection and 100 hours/week at energies for which no ramping is necessary. We give a revised estimate of days required for each remaining BES energy point to meet STAR physics goals in Table

3.2. In Run 10, we have completed our goals at 39 GeV, 11.5 GeV, 7.7 GeV, and we reached our goal for 19.6 GeV in Run 11. The remaining beam energy is 27 GeV. In addition, we support any additional work C-AD wants to do at or just above 5 GeV in Run 12.

Beam Energy (GeV)	Event Rate (Hz)	Run10 BUR request	Run 12 request	Revised estimate based on Run 10 performance
27	400	33 M	150 M	1 week

Table 3.2: BUR for 27 GeV Au+Au collisions to complete the Phase-I BES program.

From the excellent RHIC performance in Run 10 and 11, we project that we could complete our previously stated goals at 27 GeV in a few days. We do believe that in order to effectively use the collider to run an energy setup, it is much better to increase the request for the length of time at each energy to one week, the shortest amount of time we believe reasonable. The one-week run will also enhance our physics program significantly. We project that running for this amount of time will lead to much richer data samples, including measurements of hypertriton production at the 7-8 sigma level and significant signals such as the ϕ and ω in the di-lepton channel.

3.2 Physics Results to Date from Phase-I of Beam Energy Scan (BES)

There has already been a rich yield of physics from the three low energy points: 39 GeV, 11.5 GeV and 7.7 GeV, where data were taken during Run 10. Many findings have been presented outside the collaboration at conferences, and more are poised to be released at the Quark Matter conference in May, 2011.

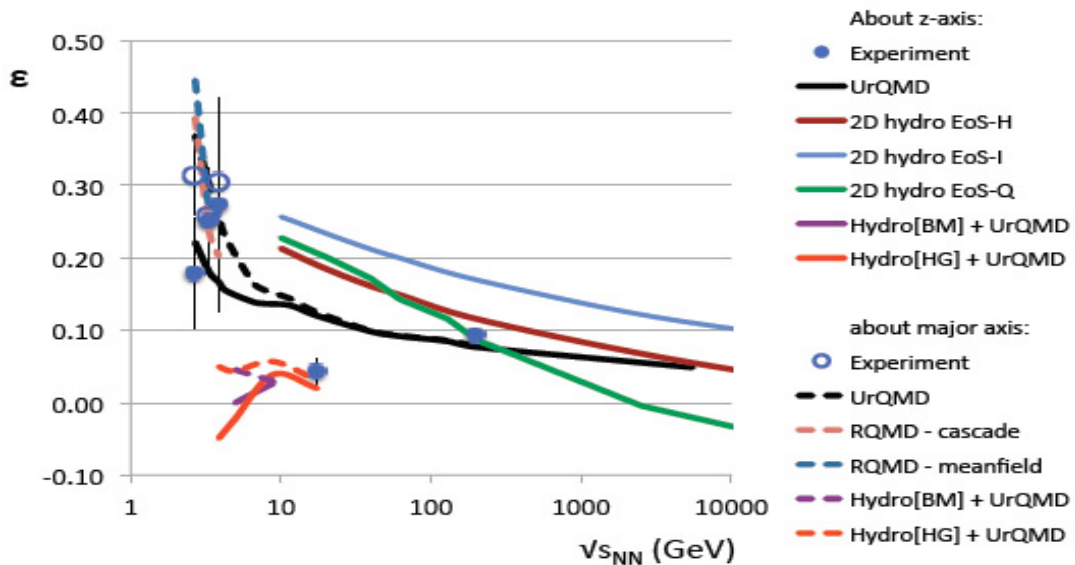


Figure 3.1: Freeze-out anisotropies for charged pions vs. beam energy, extracted from azimuthally-sensitive HBT analyses. Published measurements are shown, along with

hydrodynamic and microscopic transport calculations, based on various equations of state.

Here we summarize some findings with promise for new physics insights that have emerged so far from analyses of Run-10 data. Some of these results are quite recent and might undergo further evolution before publication.

3.2.1 Azimuthally-sensitive Hanbury-Brown Twiss Correlations

Measurements of 2nd-order oscillations in HBT radii as a function of event-plane azimuth, characterized by a final-state eccentricity ϵ , have a good sensitivity to the nuclear equation of state. Fig. 3.1 shows existing published measurements of ϵ , along with a diverse set of hydrodynamic and microscopic transport calculations, including a range of assumed equations of state [3]. The plot demonstrates the good sensitivity mentioned above, and supports the interpretation that a softening of the equation of state arising from a first-order phase transition can in principle be detected by measuring the ϵ excitation function. On the other hand, it is evident that none of the many model calculations shown consistently reproduces the published measurement, much less the more demanding constraints when the new preliminary BES measurements are included (see below).

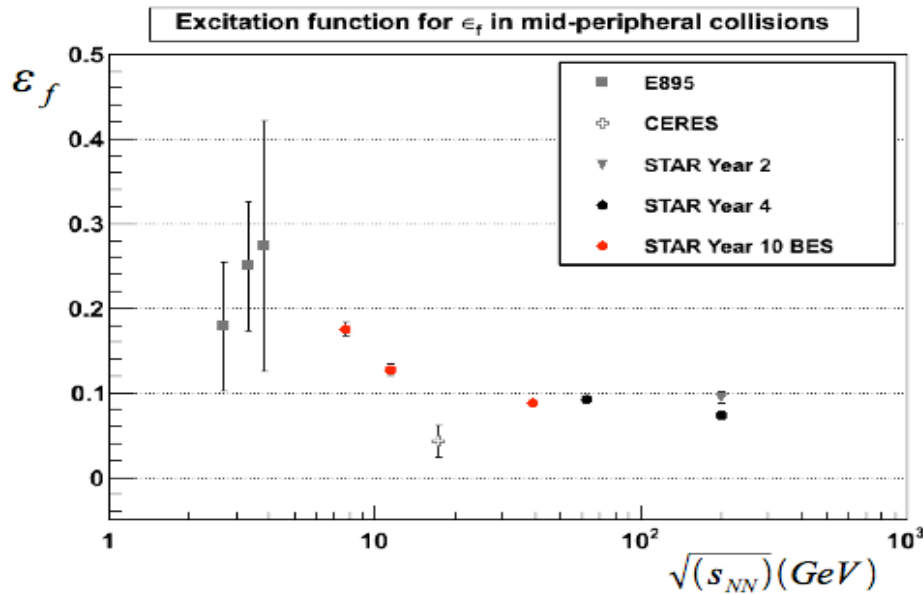


Figure 3.2: Experimental freeze-out anisotropies for charged pions versus beam energy, as extracted from azimuthally-sensitive HBT analyses, including STAR's latest preliminary BES measurements.

Fig. 3.2 shows existing published measurements of ϵ along with the new preliminary STAR measurement from run-10. The tantalizing finding is an apparent anomalous dip in ϵ at the CERES [4] energy $\sqrt{s_{NN}} = 17$ GeV. The new BES measurements from STAR make it especially difficult to reconcile the data with a smooth trend. The obvious weakness in the experimental data is the fact that different systematics might apply in

STAR and CERES and the data would clearly be more compelling if the crucial energy points 19.6 and 27 GeV could also be measured by STAR. We have just acquired the former and we propose running the latter in Run 12. Moreover, STAR can readily provide a measurement in this energy region with a much smaller statistical and systematic errors than what has been reported by CERES.

3.2.2 Constituent-Quark-Number (n_q) Scaling in Elliptic Flow

This well-known scaling behavior is one of the most striking pieces of evidence for the existence of partonic degrees of freedom during the early-stage Au + Au collision process at the highest RHIC energies. It is hard (though not impossible in all cases [5]) to explain this pattern in a scenario where only hadronic matter exists throughout the interaction, whereas the hypothesis of coalescence of hadrons from deconfined quarks offers a ready explanation. An observation of this scaling behavior turning off below some threshold beam energy would be a very powerful confirmation of our current understanding of the deconfined phase.

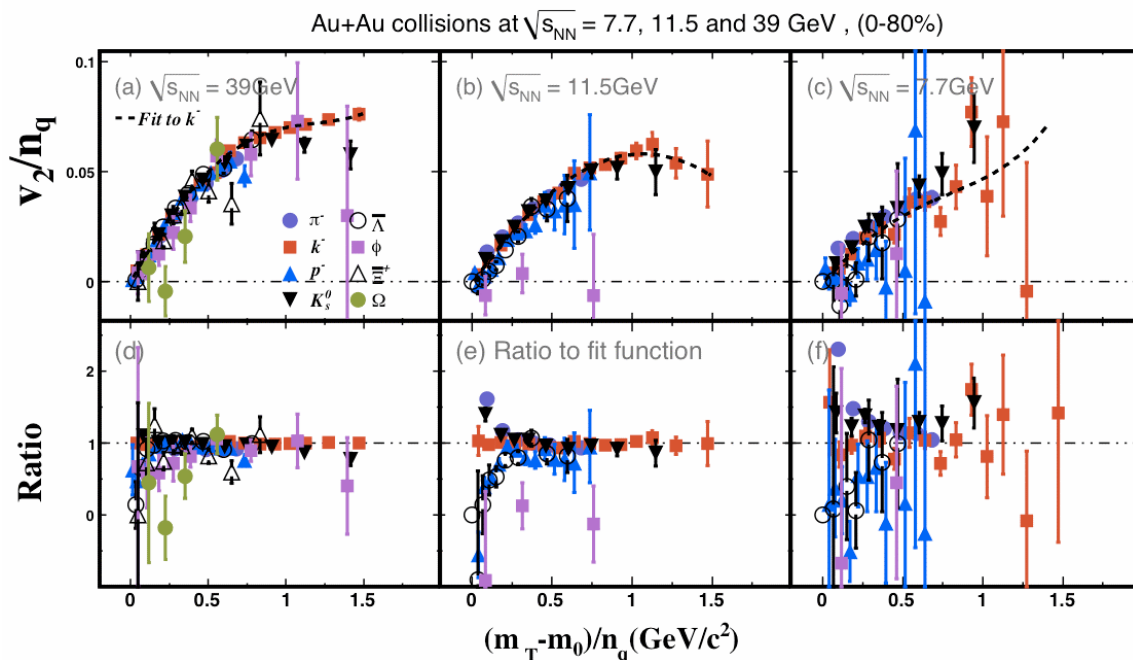


Figure 3.3: The upper row of panels presents elliptic flow per constituent quark (v_2/n_q) for various particle types indicated in the legend, vs. transverse mass (m_T) per constituent quark, for minimum-bias events at each of the three BES energies explored in run-10. The lower row shows the same data, but now plotted as a ratio with respect to a common fit function, allowing more detail to be resolved at lower m_T .

As one can see in Fig. 3.3, the remarkable feature is the ϕ -meson result at $\sqrt{s_{NN}} = 11.5$ GeV, where the data are consistent with zero flow but of course, the statistical error is larger than desirable for a highly significant conclusion. It is often argued the relatively small cross section for the ϕ to interact in the medium makes it an especially sensitive

probe of partonic degrees of freedom. If this suggestive hint of anomalous behavior has a common origin with other anomalies discussed in this section, we might expect to observe similar departures from scaling at 19.6 and 27 GeV, but with far better statistics.

3.2.3 Elliptic Flow for Baryons and Antibaryons

Figure 3.4 (left) shows elliptic flow compared between protons and antiprotons, and also between Λ and anti- Λ , for minimum bias events at the three BES energies. While baryon and antibaryon elliptic flow is in remarkably close agreement at 39 GeV, the antibaryon flow drops at 11.5 GeV and is almost consistent with being zero at 7.7 GeV. Figure 3.4 (right) shows similar data in summary form, specifically the mean fractional baryon-antibaryon difference in elliptic flow $\langle \Delta v_2 \rangle / \langle v_2 \rangle$ as a function of beam energy; for further comparison, there is a data point for 62 GeV as well as the mean fractional difference in elliptic flow for K^+ and K^- and for π^+ and π^- .

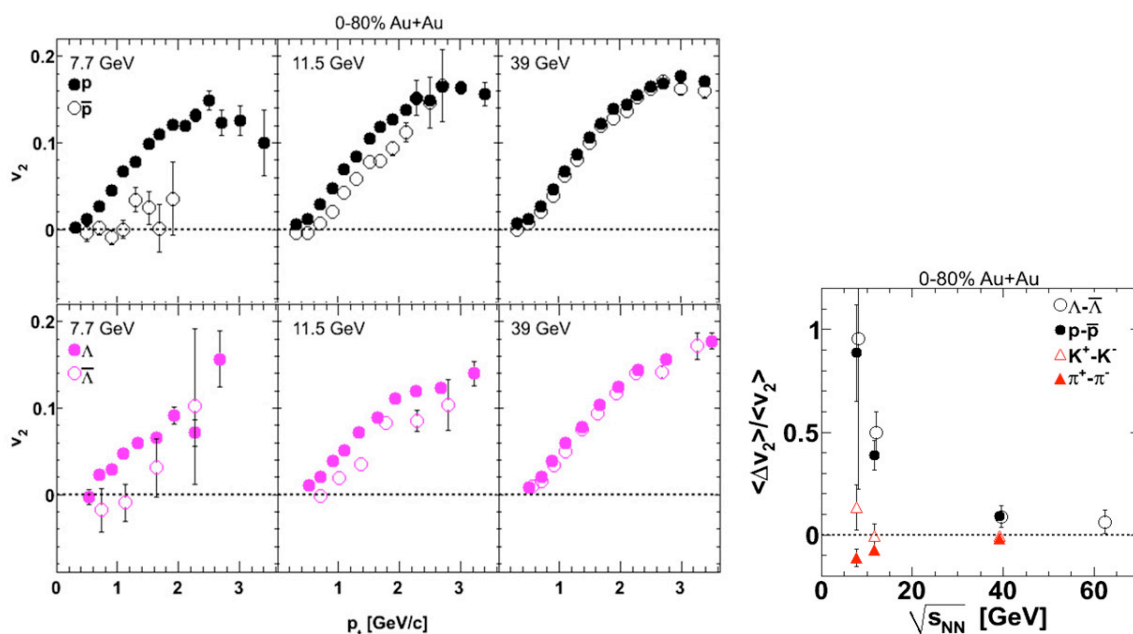


Figure 3.4: The six panels on the left show baryon and antibaryon elliptic flow vs. transverse momentum at the three BES energies from run-10. The panel on the right summarizes these data via the mean fractional baryon-antibaryon difference in elliptic flow $\langle \Delta v_2 \rangle / \langle v_2 \rangle$ as a function of beam energy, along with the same ratio for K^+ and K^- and for π^+ and π^- .

Could this striking change in behavior be connected with a change in absorption of antibaryons going from 7.7 GeV to 39 GeV, possibly due to the onset of a transition between qualitatively different early-stage media? Once again, the two missing energy points from Phase I of the BES plan, i.e., 19.6 and 27 GeV, would provide excellent statistics for an in-depth study of this anomaly in the likely region of rapidly changing absorption.

3.2.4 Directed Flow for Charged Particles and for Protons

Directed flow (v_1) can probe the onset of bulk collective dynamics. The shape of v_1 vs. rapidity is of special interest because it has been identified as a key phase transition signature [6]. At low energies, v_1 is almost directly proportional to the rapidity. In the energy range covered by the Energy Scan, directed flow is predicted to be near zero or to exhibit a pattern where v_1 changes sign three times and has a small negative slope in the vicinity of midrapidity [6].

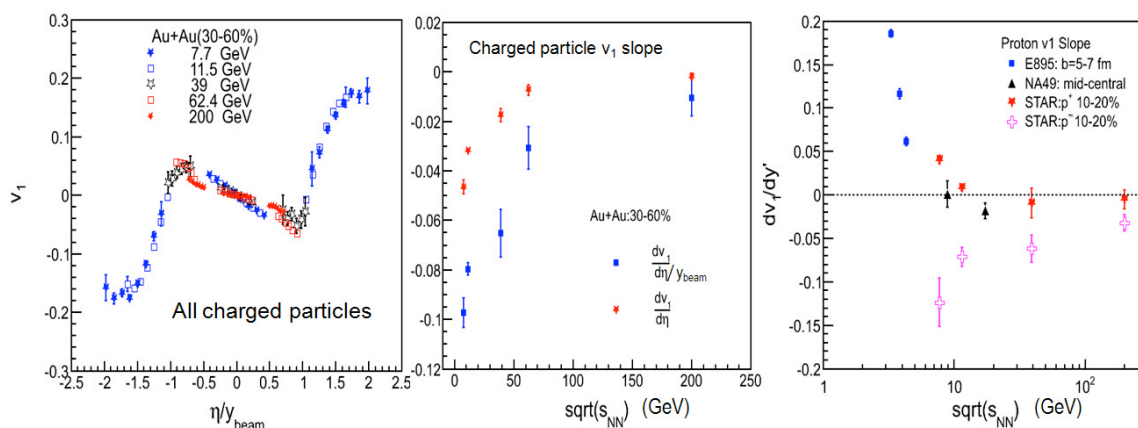


Figure 3.5: The panel on the left shows charged particle directed flow vs. pseudorapidity at available STAR energies from 7.7 GeV to 200 GeV. The x-axis is normalized by beam rapidity. The center panel shows the fitted slope $dv_1/d\eta$ in the midrapidity region, with and without this normalization, plotted vs. beam energy. The panel on the right shows normalized slope dv_1/dy' for protons and antiprotons.

Figure 3.5 summarizes some of the potentially significant features of the directed flow for all charged particles and for identified particles. The panel on the left shows charged particle directed flow vs. pseudorapidity at the three BES energies from run-10, as well as at the higher RHIC energies. The pseudorapidity axis is normalized by beam rapidity, which at higher RHIC energies causes all data to lie on a common curve. Increasing departures from this scaling are seen as the beam energy decreases in the BES region. To quantify this breaking of the scaling, the middle panel shows slopes $dv_1/d\eta$ and $dv_1/d\eta'$ near mid-pseudorapidity, where η' stands for pseudorapidity normalized by beam rapidity. There is a marked steepening of both slopes as we scan down in energy, beginning at the upper end of the BES range.

The right-hand panel of Fig. 3.5 presents normalized slope dv_1/dy' for identified protons and antiprotons. The proton slope exhibits a pattern that is totally different from that for all charged particles (dominated by pions), while the antiprotons are qualitatively more similar to all charged particles. The slopes for protons and antiprotons are highly sensitive to the centrality, and the fact that different experiments do not perfectly line-up when extrapolated is quite likely at least partly a consequence of the centrality selections not being accurately matched.

The proton slope changes sign somewhere in the region covered by the recent energy point at 19.6 and the proposed point at 27 GeV. This sign change is yet another tantalizing hint of a qualitatively different regime above and below the target range for the proposed energies to complete of Phase I of the Beam Energy Scan.

3.2.5 Correlations Related to the Chiral Magnetic Effect

There are still many open questions related to the non-trivial structure of the QCD vacuum. The generation of mass from spontaneous chiral symmetry breaking, and topological solutions (instantons, sphalerons) are relevant to this discussion. Event-by-event local parity violation in these strong interactions would be highly important new evidence that would lend support to current theoretical understanding, and would have an immediate impact, not just on relativistic heavy ion physics, but on all spheres of physics touched by QCD (high energy physics, cosmology, etc.) The observation of a local parity-violating signal assumes the following chain of circumstances. In non-central heavy-ion collisions, a large orbital angular momentum vector (L) exists at 90° to the reaction plane, leading to an exceptionally intense localized magnetic field ($\sim 10^{15}$ T, due to the net charge of the system). If the system is deconfined, there can be strong parity-violating domains, and different numbers of quarks of left- and right-handed helicity, leading to preferential emission of like-sign charged particles along L . The phenomenon is sometimes called the Chiral Magnetic Effect (CME), and has been studied in lattice QCD calculations [7].

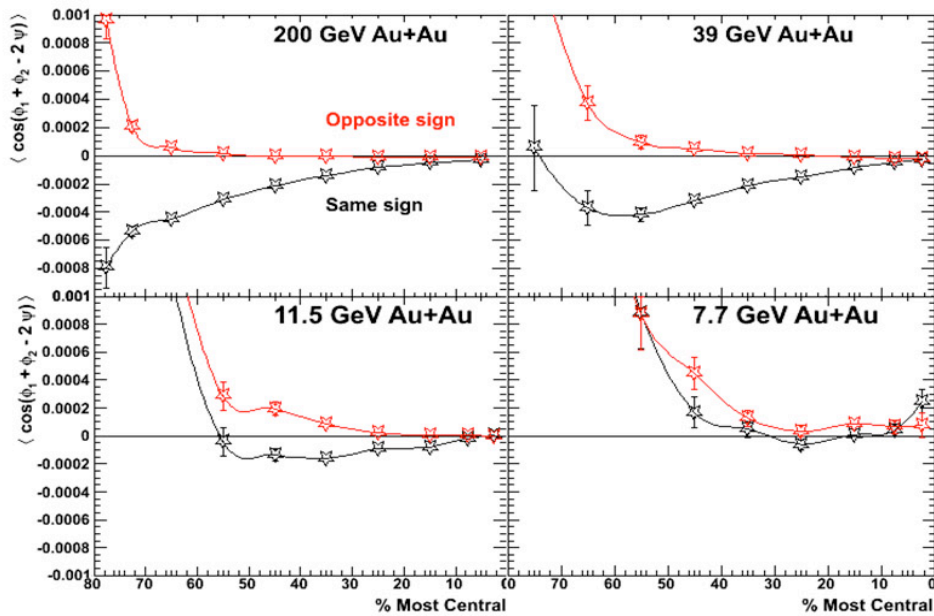


Figure 3.6: *The four panels show the evolution with energy of the correlation between pairs of particle azimuths and the reaction plane azimuth, plotted vs. centrality.*

In Fig. 3.6, at beam energies where it is believed that Local Parity Violation occurs, the plotted correlation observable shows a progressively larger difference between like- and opposite-sign charged pairs as the impact parameter increases; this is a required CME

property since the intense local magnetic field grows with impact parameter. It is widely believed that deconfinement is a necessary condition for CME observation [8], and therefore if deconfinement takes place only above a threshold energy, the signal should change accordingly. That indeed appears to happen in Fig. 3.6, and the CME signature greatly diminishes as we scan the beam energy below 39 GeV. Relatively high-statistics measurements at 19.6 and 27 GeV would help map out the crucial transition region.

3.2.6 Higher Moments and Fluctuations

It is important to understand the characteristics of the fluctuations and correlations expected in case the system passes through the region near the critical point, or in case it passes through a first-order phase transition. Those correlations and fluctuations must be disentangled from backgrounds such as resonance decays, jet fragmentation, elliptic flow, and other sources of correlations not related to the critical point. The characteristic signature of the existence of a critical point is an increase, and divergence, of fluctuations. Lattice QCD calculations indicate large jumps in the baryon, charge, and strangeness susceptibilities as a function temperature of the system. These susceptibilities can be related to event-by-event moments of various observables in heavy-ion collisions, in particular to fluctuations of conserved quantities (net charge, net baryon and net strangeness).

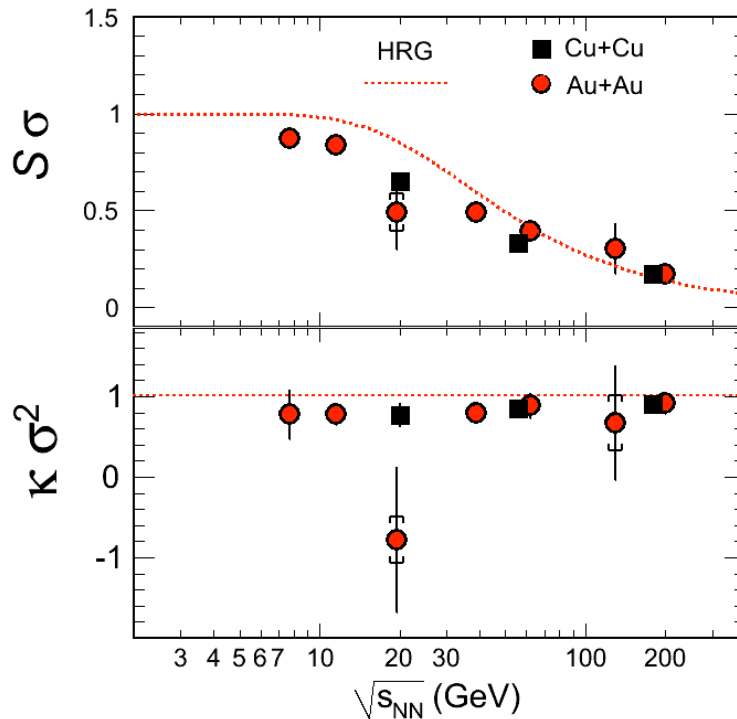


Figure 3.7: These two panels show the beam-energy dependence of fluctuation observables $S\sigma$ and $\kappa\sigma^2$, related to skewness and kurtosis, respectively. The dotted curves correspond to calculations from the Hadron Resonance Gas (HRG) model.

The moments S (skewness) and κ (kurtosis) involve the third and fourth power, respectively, of the deviation from the mean, and reflect departures from a Gaussian distribution. When they are multiplied by the appropriate power of σ (the standard deviation), the desirable characteristic of minimum sensitivity to multiplicity is obtained. Fig. 3.7 though still preliminary, is consistent with other studies in suggesting that beam energies near 39 GeV and below are important for further study.

3.3 Summary of Noteworthy Preliminary Result from the Beam Energy Scan

The STAR Beam Use Request submitted in 2009 laid out the overall plan for Phase-I of the Beam Energy Scan (BES), which entails a fairly coarse survey of the full energy range accessible to the RHIC machine – specifically, a scan over the six energy points 39, 27, 19.6, 11.5, 7.7 and 5 GeV. Run-10 successfully covered three of these six energy points, and target statistics were reached or exceeded at each energy point. Even with BES Phase-I only half analyzed, a rich and detailed phenomenology is emerging, and prior concerns that the new measurements might be consistent with just a smooth interpolation between existing results at higher and lower energies have proven groundless. There is a remarkably diverse set of independent measurements – including femtoscopy parameters, elliptic flow of ϕ -mesons and of antibaryons, directed flow of charged particles and of protons, correlations associated with the Chiral Magnetic Effect, and higher-moment fluctuation observables – all offering indications of qualitative changes in the collision process within the coverage of the Beam Energy Scan, and in particular, the missing region covered by 27 GeV appears to be especially interesting and deserving of special scrutiny.

References:

- [1] M. Asakawa *et al.*, Phys. Rev. Lett. **101**, 122302 (2008).
- [2] R. V. Gavai and S. Gupta, Phys. Rev. **D78**, 114503 (2008).
- [3] M.A. Lisa, E. Frodermann, G. Graef, M. Mitrovski, E. Mount, H. Petersen and M. Bleicher, preprint (to be posted soon on arXiv).
- [4] D. Adamova *et al.* (CERES collaboration), Phys. Rev. C **78**, 064901 (2008).
- [5] Y. Lu, M. Bleicher, F. Liu, Z. Liu, H. Petersen, P. Sorensen, H. Stoecker, N. Xu, X. Zhu, J. Phys. G **32**, 1121 (2006).
- [6] R. Snellings *et al.*, Phys. Rev. Lett. **84**, 2803 (2000); J. Brachmann *et al.*, Phys. Rev. C **61**, 024909 (2000); L. P. Csernai and D. Rohrlich, Phys. Lett. B **458**, 454 (1999); H. Stoecker, Nucl. Phys. A **750**, 121 (2005).
- [7] P. V. Buividovich, M. N. Chernodub, E. V. Luschevskaya and M. I. Polikarpov, Phys. Rev. D **80**, 054503 (2009); M. Abramczyk, T. Blum, G. Petropoulos and R. Zhou, arXiv:0911.1348; P. V. Buividovich, E. V. Lushchevskaya, M. I. Polikarpov and M. N. Chernodub, JETP Lett. **90**, 412 (2009).
- [8] D. Kharzeev, Phys. Lett. B **633**, 260 (2006); D. E. Kharzeev, L. D. McLerran and H. J. Warringa, Nucl. Phys. A **803**, 227 (2008).

3.4 Physics of 200 GeV U+U Collisions at RHIC

3.4.1 Introduction

The commissioning of the EBIS upgrade will enable Uranium beams to be accelerated at RHIC. The prolate shape of Uranium opens up a new horizon of measurements at RHIC, in which we can study the interplay of nontrivial geometrical configurations of the collision zone against fluctuations in those geometrical configurations.

Grazing (non-central) collisions of spherical nuclei produce overlap areas predominantly of elliptic shape, in which the second Fourier coefficient dominates. The interactions in and expansion of the spatially asymmetric fireball lead to large asymmetries in momentum space. Since the spatial asymmetry quickly washes out, the observed momentum space asymmetries are a sensitive probe of the early dynamics of the expanding system. These anisotropies are quantified by the various coefficients in the Fourier expansion of the azimuthal distribution of the transverse momenta (or number of particles). The second coefficient, v_2 , is a measure of anisotropy arising due to the elliptic shape of the overlap zone, and has been found over the past decade to be large and the dominant coefficient.

Attention has turned in recent years towards the effects of fluctuations in the shape of the initial overlap zone, rather than the smooth event-averaged shapes in earlier studies. Depending on the size and number of constituents that create the zone (whether nucleons, as implemented in a Monte Carlo Glauber model, or some other constituent as implemented in Color Glass Condensate-inspired models such as fKLN), the overlap zone can have strong higher-order coefficients that fluctuate event-by-event. Since interactions act in a given event, these fluctuations can lead to fluctuations in the final-state momentum distributions, and appear in the two- and higher-order particle correlations that are used to measure v_n . In head-on (central) collisions of spherical nuclei, in which the event-averaged shape is nearly spherical, these fluctuations can be the dominant source of the measured v_n . These fluctuations are also a leading counter-explanation for two-particle correlation structures in central collisions, such as long-range correlations in rapidity (“ridges”) and at relative azimuthal angles away from 180 degrees (“conical flow”), which had previously been attributed to the reaction of the QCD medium to penetration by a jet, or to modifications of the jet properties themselves by the medium. Distinguishing which explanation is correct is still an active area of debate, and has the potential to produce a much broader range of constraints on the properties of the medium (and potentially at what length scale [1]) than can be done by event-averaged methods alone.

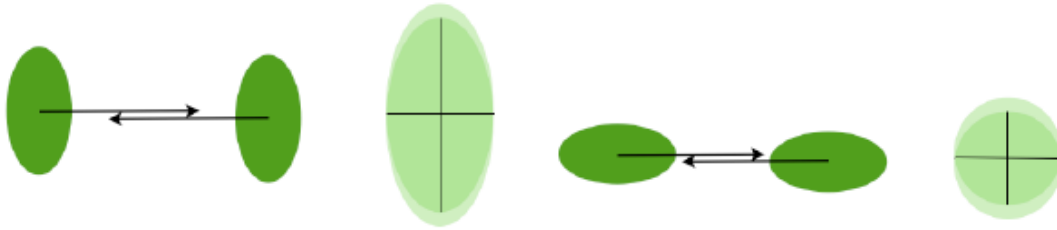


Figure 3.8: Schematic of body-body (left two) vs tip-tip (right two) U+U collisions, with the left figure of each pair in the x-z plane and the right in the transverse plane.

In contrast to central Au+Au collisions, because of the prolate shape of Uranium, there are configurations (body-body) in which central U+U collisions are not spherical in the transverse plane, but have a strong event-averaged elliptic shape. These configurations are a subset of all possible configurations, since collisions can occur at all possible relative angles of the two incoming Uranium nuclei. In some sense, these angles introduce an additional source of fluctuation in central U+U collisions relative to central Au+Au collisions, but the fluctuations due to angles are at a much larger length scale than the fluctuations due to the constituents. They are also amenable to characterization with global measures such as multiplicity and Zero Degree Calorimeters. Central U+U collisions of all orientations can be selected by requiring a small energy in the forward direction, indicating no (or few) neutron spectators. Within this set of events, more spherical events can be selected as those with higher multiplicity, since as more spherical configurations in the transverse plane involve longer paths of interaction in the longitudinal direction, and so a higher number of binary collisions. This correlation between multiplicity and geometry has been studied in both Monte Carlo Glauber and fKLN implementations, and is robust [2].

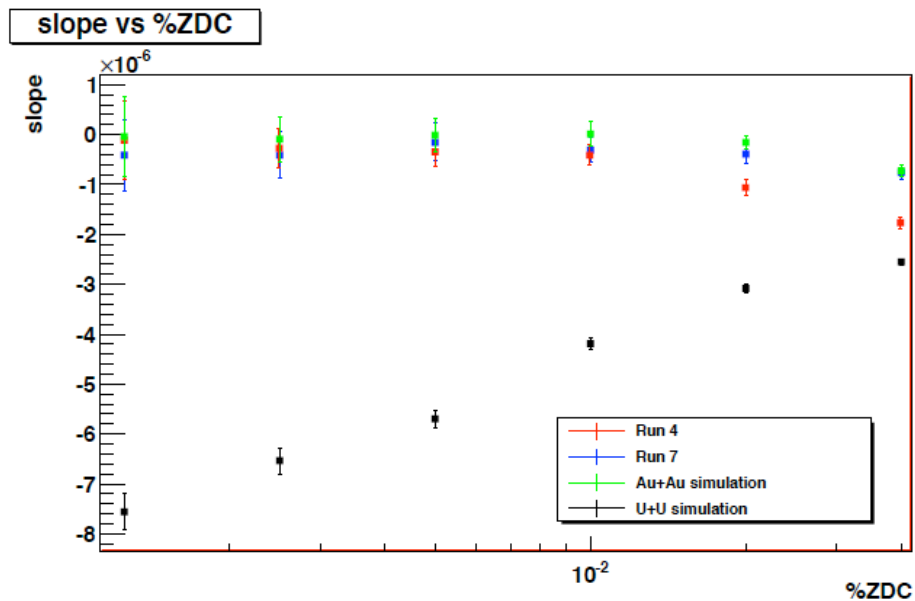


Figure 3.9: Benchmarking of ability to select geometries in U+U collisions. Vertical axis is the slope of measured v_2 vs. multiplicity, dv_2/dM , while the horizontal axis is the

percent of the total ZDC cross section contained below an upper cut in ZDC energy. Results of analysis in data are indicated by “Run 4” and “Run 7”.

STAR has benchmarked its ability to select these event configurations with both Monte Carlo Glauber calculations, and with the application of these techniques to real Au+Au events from Runs 4 and 7. The data sample is first selected in tight bins in ZDC energy, in each bin of which v_2 is studied vs. multiplicity (M), and a slope dv_2/dM obtained. As shown in Figure 2, in Au+Au collisions, one expects dv_2/dM to approach zero when one is solely selecting on fluctuations, both physically and due to detector response. This behavior is seen, and the details of the approach towards a slope of 0 for decreasing upper cut in ZDC energy is well simulated. In contrast, from the same calculations, the slope is expected to be large, negative, and increasing in absolute magnitude with decreasing cut in ZDC energy in U+U collisions. The behavior in U+U collisions should be easily distinguishable from that in Au+Au collisions.

Beyond investigating geometry and hydrodynamic behavior, the grossly deformed overlap zone will enable investigations in several other important areas; the path-length dependence of energy loss ($dE/dx(L)$), Local Parity Violation (LPV) and Ultra-Peripheral Collisions (UPC)

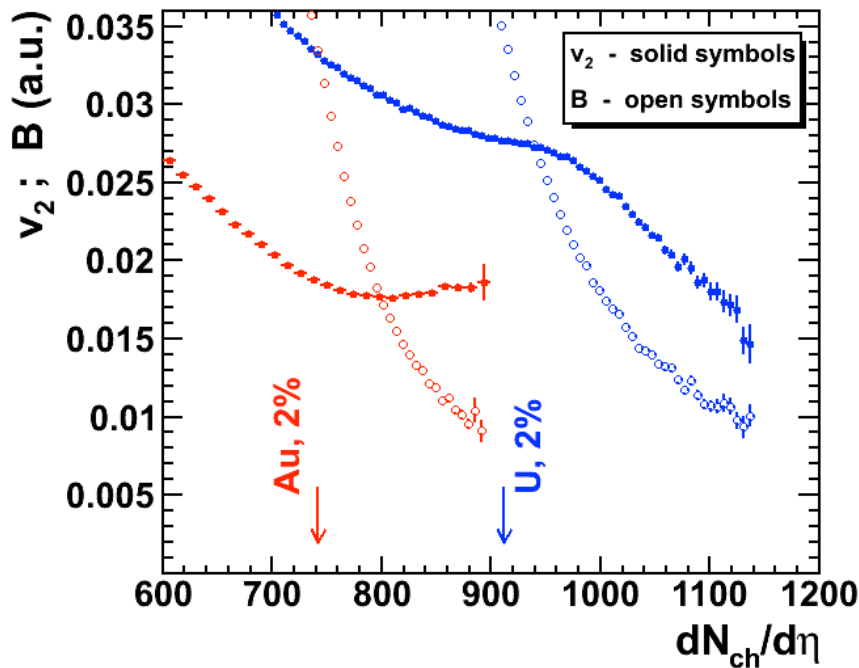


Figure 3.10: Magnetic Field and v_2 vs. multiplicity density $dN_{ch}/d\eta$. Fig. from [5].

$dE/dx(L)$: Current theories of energy loss for fast partons assume a non-linear dependence on path-length, but this has not yet been fully tested in experiment, partially because of the small difference in path lengths for the parton traversing in plane and out of plane. Body-body U+U collisions are expected to provide almost twice as much

difference between the in plane and out of plane path lengths for the same eccentricity as semi-peripheral Au+Au collisions. With modest data samples, these path length effects can be investigated via single-hadron and di-hadron suppression, as done in RHIC Runs 1,2, and 4. More detailed investigations utilizing rarer probes await high luminosity running.

LPV: Parity is conserved in the strong interaction, but local parity violation has long been expected because of the topological structure of QCD. A signal of local parity violation, from the Chiral Magnetic Effect [3] and the strong QED magnetic field in non-central collisions, may have been observed in high-energy nuclear collisions [4]. Since the observable used is parity even, there is a possibility that more mundane processes can mimic the signal of local parity violation. The magnetic field required for the parity-violating signal can only exist in non-central collisions, as it is produced mainly by the spectators as they travel from the collision zone. In fully central U+U body-body collisions, there are no spectators, while in certain configurations the geometry of the collision zone induces v_2 . The signal from true local parity violation should therefore be small, while possible backgrounds should remain strong. One therefore can use the U+U body-body collisions, where the field should be small or zero, to further test if the observations in Ref. [4] originate from local parity violation or more mundane background processes.

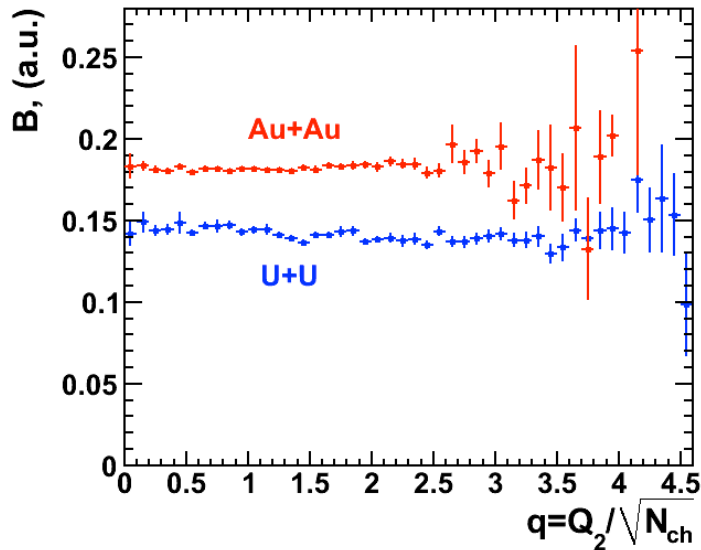


Figure 3.11: *Dependence of the magnetic field strength on the flow vector q for events with fewer than 20 spectators. Figure from [5].*

As shown in Figure 3.10 from Ref. [5], distinguishing tests can be done even without double selection on ZDC signal and multiplicity. The figure shows the QED magnetic field strength, along with predicted v_2 , as a function of multiplicity alone, from a Glauber calculation. The behavior of v_2 with multiplicity is rather different between Au+Au and U+U, with U+U showing a distinct knee at multiplicity 1000, beyond which higher multiplicity selects more spherical configurations. In contrast, the dependence of the magnetic field strength on multiplicity is very similar between Au+Au and U+U once the

overall multiplicity scale is matched. Background processes are expected to be closely related to v_2 , while the signal from local parity violation is expected to be closely related to the magnetic field strength.

If one can select at small enough ZDC energy, the magnetic field and v_2 can potentially be completely decoupled, as seen in Fig. 3.11, which from the same model plots the magnetic field vs. the flow vector magnitude q , for events with less than 20 spectators. For this set of events, while the flow vector magnitude is strongly correlated to v_2 (and can be used as a measure of v_2 event by event), the magnetic field shows no dependence on q . One can study in data the measures sensitive to local parity violation vs. the flow vector q ; any dependence indicates contamination from processes not related to the Chiral Magnetic Effect. The cut in ZDC for this plot is a relatively loose cut, as compared to the cuts discussed in the earlier section, selecting 1.5% of the events in U+U collisions and 2.3% in Au+Au. These studies should therefore be feasible with a sufficiently large data sample.

UPC: The unique geometry of U+U collisions also opens up an exciting possibility in Ultra-Peripheral Collisions studies. These studies are based in coherent phenomena across the entire nucleus, which can be affected significantly by quantum correlations. The geometry of U+U collisions can enhance the probability for multiple vector meson production and multi-photon interactions to occur. Based on the production rates for single and double ρ production [6] and assuming the cross-section scales as $Z^8*[A^{5/3}]^2$, about 1 out of 1,000 ρ^0 should be accompanied by a second ρ^0 . Such multi- ρ samples enable the study of quantum correlations in production and decay, in which stimulated decay is a possibility.

3.4.2 Run 12 U+U at 200 GeV Request

The physics of U+U collisions can be split into two distinct classes, which have distinct requirements for beam conditions. The first class consists of bulk observables, such as multiplicity, elliptic flow, HBT, and the like. These have relatively small requirements in terms of the number of events, and are mainly focused on hydrodynamic behavior of the medium, though some measurements related to hadron quenching in medium can be made with such samples (as in the first years of RHIC Au+Au). This class also contains the light vector meson portion of the Ultra-Peripheral Collision program.

The second class of measurements consists of rare, triggered probes, such as γ -hadron, jets, and heavy flavor suppression, which are extremely luminosity hungry. Due to the large configuration space for the relative orientation of the two U nuclei at the collision point, restrictive cuts on data samples need to be made in order to select the most interesting densities and geometries. As shown in Fig. 3.9, even in Au+Au collisions we have a non-zero slope in dv_2/dM for a ZDC cut that includes 0.5% of the cross section, and expect to have sensitivity for tighter cuts in U+U collisions. Such a cut, combined with 5-10% cuts on multiplicity, decreases sample sizes from minimum bias by a factor of a few thousand. This implies that rare probes need high luminosities, which may not be achievable in Run 12.

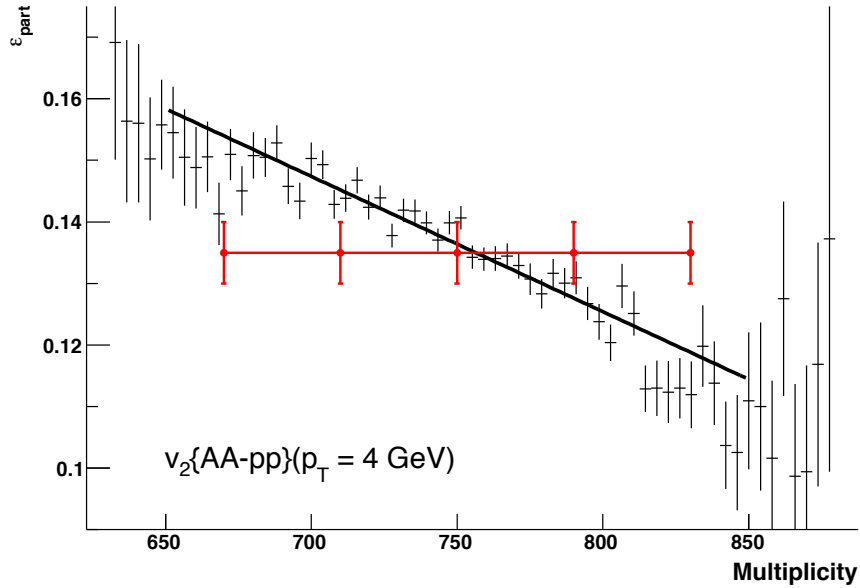


Figure 3.12: *Black:* $\langle \epsilon_{part} \rangle$ as a function of measured mid-rapidity multiplicity in the most 1% central U+U collisions, as selected by the number of participants. *Red:* estimated uncertainties on $v_2\{AA-pp\}$ for $p_T=4 \text{ GeV}/c$ for such events, as selected with the ZDCs.

With DAQ1000 and a modest collision rate of 5-10 kHz, we estimate that STAR can accumulate 400M events, approximately half central and half minimum bias, in six weeks' time. The central trigger will likely be based on the number of spectator neutrons seen in the ZDC, which has single-neutron resolution and has been used successfully in all previous Au runs as a centrality trigger. The precise selection of centrality fraction in this trigger will depend on available collision rates.

Such a sample should allow for sufficiently fine-grained selection of geometries to investigate the behavior of v_2 , HBT with respect to the reaction plane, and related measurements. It will also allow for some measurements related to jet quenching, such as suppression of single-hadron spectra and di-hadron correlations, at accuracies approximately at the level investigated in Au+Au collisions in Runs 2 and 4.

Examples of statistical uncertainties for two processes of interest are shown in Fig. 3.12 and 3.13. Fig 3.12 shows the projected v_2 at p_T of 4 GeV/c, as a function of multiplicity in the 1% most central collisions as determined by the spectator neutrons in the ZDCs. With 200M 0-10% central ZDC events, each multiplicity bin contains approximately 2M events, and so has equivalent statistics to the Run 2 central data set. Also shown on the figure is a calculation of the expected change in v_2 over this range in multiplicity, as estimated from the participant eccentricity ϵ_{part} as calculated in a Monte Carlo Glauber model. Fig. 3.13 shows the projected accuracy of R_{AA} for $p_T > 6 \text{ GeV}/c$, again as a function of multiplicity for the 1% most central collisions as selected by the ZDCs, along with the possible range over which R_{AA} may be expected to vary. In both cases,

statistical accuracies are sufficient to assess the level to which the cuts select on the geometry of the collision, rather than on fluctuations.

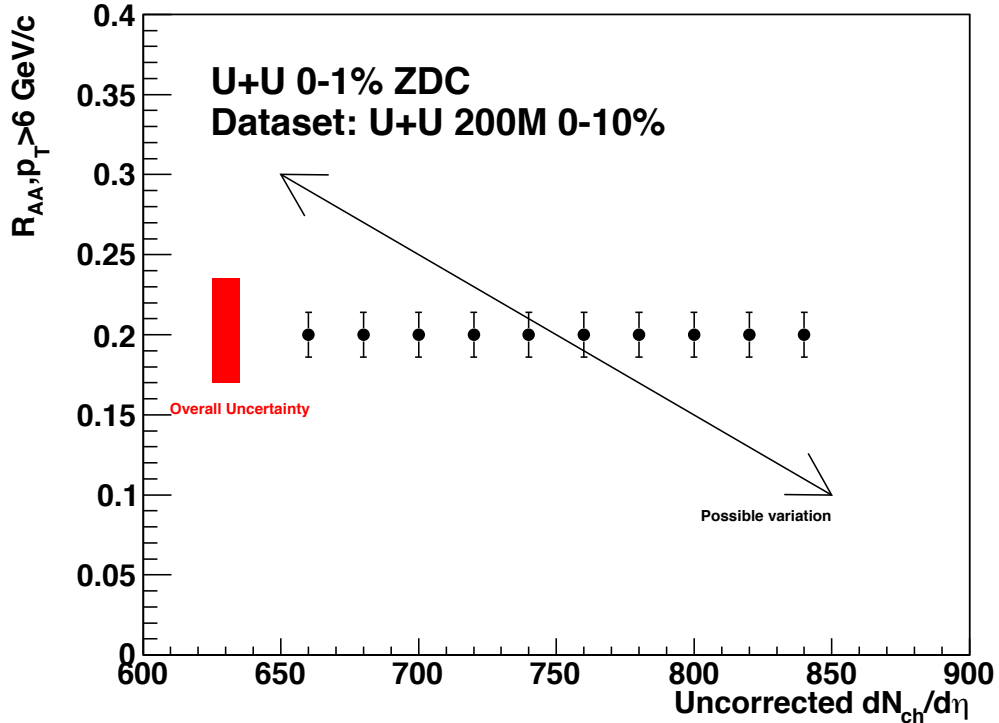


Figure 3.13: Projected R_{AA} as a function of measured mid-rapidity multiplicity for the 1% most central collisions, as selected with the ZDCs. Red box shows overall uncertainty, common to all points, while error bars show point-to-point uncertainty, dominated by statistical uncertainty. Arrow shows possible range of variation across this multiplicity range.

The main purpose of the U+U run in Run 12 is to better understand entropy production and possible saturation effects in A+A collisions and to establish the level to which unique geometric configurations can be selected beyond fluctuations. We need a sufficient dataset to see statistically significant variation in physical quantities, such as R_{AA} and v_2 , in order to find the point at which fluctuations dominate over physical variations. At somewhat coarser granularity in geometrical selection, signals of local parity violation can be studied. We estimate that such a dataset will take six weeks to obtain. For this first run, slightly lower energy beams are acceptable, as may be necessary with the lower Z/A of U vs. Au, but for precision high luminosity tests in the future it would be preferable to match energies with other collision systems.

References:

- [1] P. Sorensen, A. Moczy, arXiv:1008.3381.
- [2] A.J. Kuhlman and U.W. Heinz, Phys. Rev. **C72**, 037901(2005);
U.W. Heinz and A.J. Kuhlman, Phys. Rev. Lett. **94** 132301(2005);
A.J. Kuhlman, U.W. Heinz, and Y. Kovchegov, Phys. Lett. **B638**, 171(2006).
- [3] D. Kharzeev, R. D. Pisarski and M. H. G. Tytgat, Phys. Rev. Lett. **81**, 512(1998) and

references therein.

[4] B.I. Abelev, et al., (STAR Collaboration), Phys. Rev. Lett. **103**, 251601(2009); *ibid*, Phys. Rev. C, in Print, 2010; arXiv: 0909.1717 [nucl-ex].

[5] S. Voloshin, Phys. Rev. Lett. **105**, 172301 (2010).

[6] S. Klein and J. Nystrand, Phys. Rev. **C60**, 014903(1999).

4. Study of p+p Collisions

4.1 Introduction

The STAR spin physics program studies proton spin structure in terms of quarks and gluons, and the dynamics that underlie transverse spin phenomena observed in proton collisions at forward pseudo-rapidities. This program is complemented by polarized elastic scattering measurements with Roman Pots, which enable also the study of central particle production in scattering that leaves the beam protons intact (e.g. double-Pomeron exchange).

To advance the STAR spin physics program we request 12 weeks of polarized proton-proton operations at $\sqrt{s} = 500$ GeV in Run 12. Such a request would serve continued commissioning and development of RHIC luminosity, polarization, and polarization measurement. The STAR Forward GEM Tracker (FGT) is currently being assembled, and it will be installed prior to Run 12. The FGT will enhance the forward tracking capabilities, targeted primarily for charged-sign discrimination of high- p_T tracks of electrons (positrons) from $W^{-(+)}$ decays. The STAR collaboration has recently published results of $W^{-(+)}$ production at mid-rapidity [1]. The Run 12 data sample will allow significant improvement of the mid-rapidity ($-1 < |\eta| < 1$) measurement of the longitudinal single-spin asymmetry A_L for $W^{-(+)}$ production and subsequent leptonic decay. The installation of the FGT will extend the mid-rapidity measurements into the forward/backward rapidity ($(1 < |\eta| < 2)$) region.

The integrated luminosities in our request are based on the RHIC Collider Projections (FY2011 - FY 2015) document of May 11, 2010 [2]. Recent guidance from W. Fischer [3] indicates that we should take the actual performance from Run 11 as the minimum expectation for Run 12, together with the maximum projection for Run 12 quoted in the May, 2010, document. This implies the delivered luminosity for 12 weeks could fall anywhere between 140 and 500 pb^{-1} . The normal STAR procedure assumes the mid-point of the projected minimum and maximum delivered integrated luminosities for planning purposes. We scale the delivered luminosity by 60% to account for the anticipated STAR data sampling efficiency. We note that the extraordinarily wide band between the minimum and maximum projections for Run 12 makes this procedure far more uncertain this year than it has been in the past. This procedure implies that STAR might sample approximately 190 pb^{-1} during the 12-week period. This entire sampled luminosity will contribute to STAR measurements of A_{LL} for jets and di-jets to extend our knowledge of gluon polarization to lower values of x . 90-95% of this sampled luminosity will also be available for mid-rapidity measurements of A_L for W production, because of the additional dead time associated with the BEMC. Approximately 170 pb^{-1} will be sampled after the FGT commissioning is completed, and will also be useful for measurements of A_L for W production at forward rapidities. For simplicity, we assume 170 pb^{-1} for W s across the full rapidity region that STAR can observe. We consider it essential for the success of the $\sqrt{s} = 500$ GeV longitudinal spin physics program to measure (anti-)quark polarizations and gluon polarization that proton beam polarizations of at least 50% are achieved routinely and reproducibly during physics production

running during Run 12. Precision in $W^{(+)}$ asymmetry measurements and in measurements of $\Delta g(x)$ at $\sqrt{s} = 500$ GeV can be achieved with 300 pb^{-1} sampled luminosity and 70% beam polarization, and forms a multi-year goal.

4.2 Recent Results from 200 GeV p+p Collisions during Run 9

At the recent DIS 2011 conference, STAR released new preliminary results on A_{LL} for inclusive and di-jet production in 200 GeV p+p collisions, based on the data that were recorded during Run 9. Figure 4.1 shows the Run 9 measurement of A_{LL} for inclusive jets [4] over the range $|\eta| < 1$, together with the Run 6 inclusive jet A_{LL} measurements for $-0.7 < \eta < 0.9$ and model predictions from GRSV and DSSV. Figure 4.2 shows the Run 9 measurement of A_{LL} for di-jets [5] for three different pseudo-rapidity regions, compared to model predictions from GRSV, DSSV, and GS-C. The inclusive jet results are derived from $\sim 20 \text{ pb}^{-1}$ of data. The di-jet results are derived from $\sim 10 \text{ pb}^{-1}$. The average polarization was $\sim 58\%$. Both measurements profited from improvements in the jet patch trigger prior to Run 9 that increased the acceptance by nearly 40%, and from reductions in the jet patch threshold, and hence increased jet efficiency, enabled by DAQ1000.

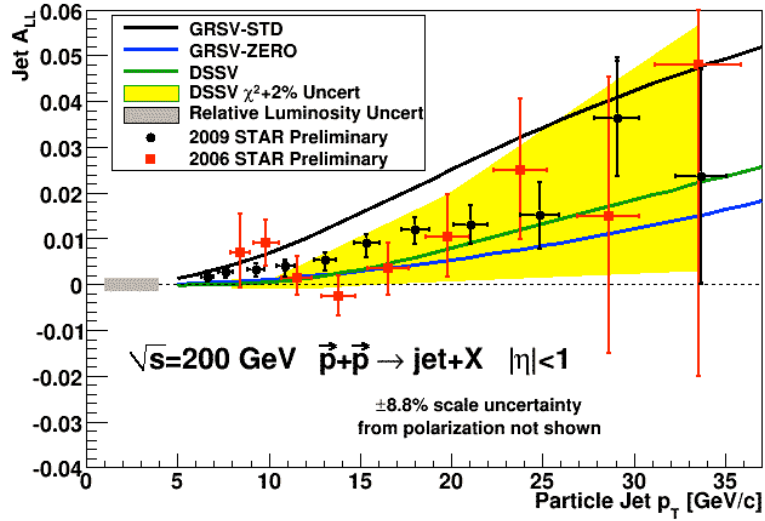


Figure 4.1: Preliminary results for A_{LL} vs. p_T for inclusive jets in 200 GeV p+p collisions from Run 9. The Run 9 results for $|\eta| < 1$ are compared to previous Run 6 results for $-0.7 < \eta < 0.9$, and to model predictions from GRSV-STD, GRSV-ZERO, and DSSV. The yellow band shows the $\chi^2+2\%$ uncertainty band for inclusive jet A_{LL} derived from the DSSV fit. Taken from [4].

These two Run 9 measurements are important complements to each other. The high precision of the inclusive jet result will lead to a significant reduction in the uncertainty in ΔG , as indicated by the narrow band that the results track through the $\chi^2+2\%$ DSSV uncertainty band shown in Fig. 4.1. However, each inclusive jet data point integrates over a broad range of gluon x values. Thus, the inclusive jet results need to be included in a global analysis to achieve their full discriminating power. In contrast, the di-jet measurement allows event-by-event determinations of x_1 and x_2 at leading order. Thus,

the di-jet measurement will provide a direct experimental constraint on the shape of $\Delta g(x)$, which will reduce the uncertainty on extrapolations of the gluon polarization beyond the currently measured region.

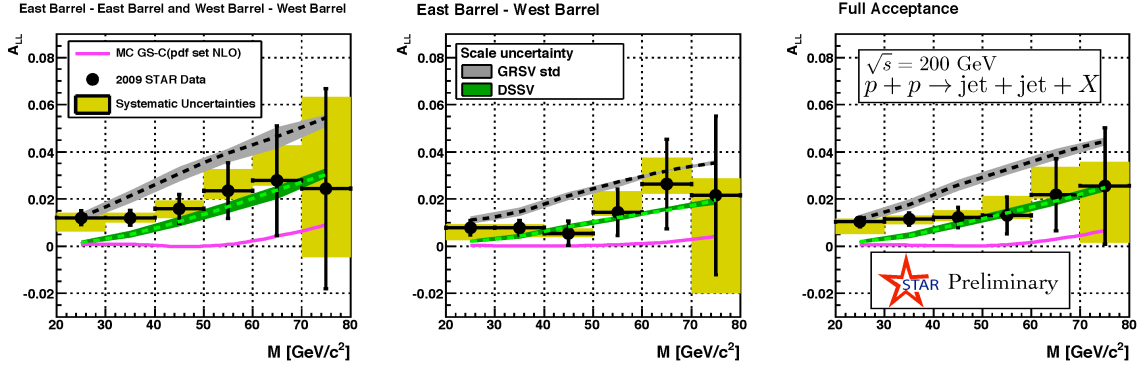


Figure 4.2: Preliminary results for A_{LL} vs. Mass for di-jets in 200 GeV $p+p$ collisions from Run 9. Also shown are model predictions from GRSV-STD, DSSV, and GS-C. The left panel shows the results for events where both jets fall into the region $0 < \eta < 0.8$ or both jets fall into the region $-0.8 < \eta < 0$, which emphasizes asymmetric partonic collisions. The middle panel shows the results for events where one of the jets falls into the region $0 < \eta < 0.8$, while the other falls into the region $-0.8 < \eta < 0$, which emphasizes symmetric partonic collisions. The right panel shows the combined result. Taken from [5].

The Run 9 inclusive and di-jet results are a factor of 3 or greater more precise than the analogous Run 6 results. The two measurements provide a consistent picture, indicating that the gluon polarization falls between the predictions from DSSV and GRSV-Std. To obtain an initial idea of their possible implications, we have performed simple fits of the inclusive jet results to an interpolation between GRSV-ZERO and GRSV-STD. An excellent description of the data is obtained with a gluon polarization equal to about 20% of the proton spin. This is small compared to early conjectures that invoked the axial anomaly, with $\Delta G > 1$, to explain the small $\Delta\Sigma$ found in inclusive deep-elastic scattering. But this can't be considered small in any absolute sense, as it implies the gluon contribution to the proton spin is likely of the same order as the quark contribution.

4.3 Performance and Experience from Run 11

Polarized proton-proton operations in Run 11 at $\sqrt{s} = 500$ GeV served continued collider and experiment development, and aimed at sampling an integrated luminosity of $\sim 20 \text{ pb}^{-1}$ with $\sim 40\text{-}45\%$ transverse polarizations in 4-5 weeks, followed by $\sim 100 \text{ pb}^{-1}$ with $\sim 50\%$ longitudinal beam polarizations in 6-5 weeks (10 weeks total). These goals were based on the projected RHIC performance in Run 11 [2], reproduced in Figure 4.3, and a STAR sampling efficiency of $\sim 60\%$. The STAR transverse goals aimed at measurements of the transverse single spin asymmetry A_N for π^0 and η mesons produced at forward pseudo-rapidities. Following expedient commissioning of the STAR Forward Meson Spectrometer (FMS) at $\sqrt{s} = 500$ GeV, a total integrated luminosity of 24 pb^{-1} was sampled with transverse beam polarizations. Figure 4.4 shows the hydrogen-jet measured beam polarizations during Run 11. STAR has thus convincingly reached its Run 11

transverse physics goals. Offline analyses of these data will commence shortly. Multiple weeks of RHIC downtime and luminosities at the lower end of the projections have prevented STAR from obtaining a data sample with longitudinal beam polarizations in Run 11 that would allow a qualitative extension of physics results beyond those obtained from Run 9. The STAR commissioning goals, including in particular scaler-based local polarimetry, were achieved.

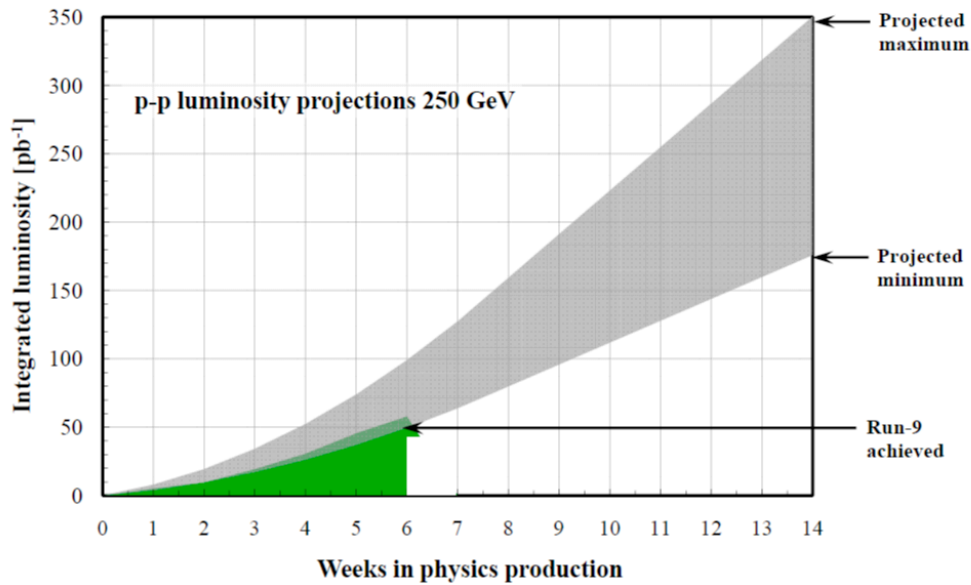


Figure 4.3: RHIC Run 11 polarized proton luminosity projections for 250 GeV running. The expected store polarization was 35-55% and average store luminosity is up to $100 \times 10^{30} \text{ cm}^{-2} \text{ s}^{-1}$. These estimates assumed that peak performance would be reached after 8 weeks of linear ramp-up, starting with 25% of the final value.

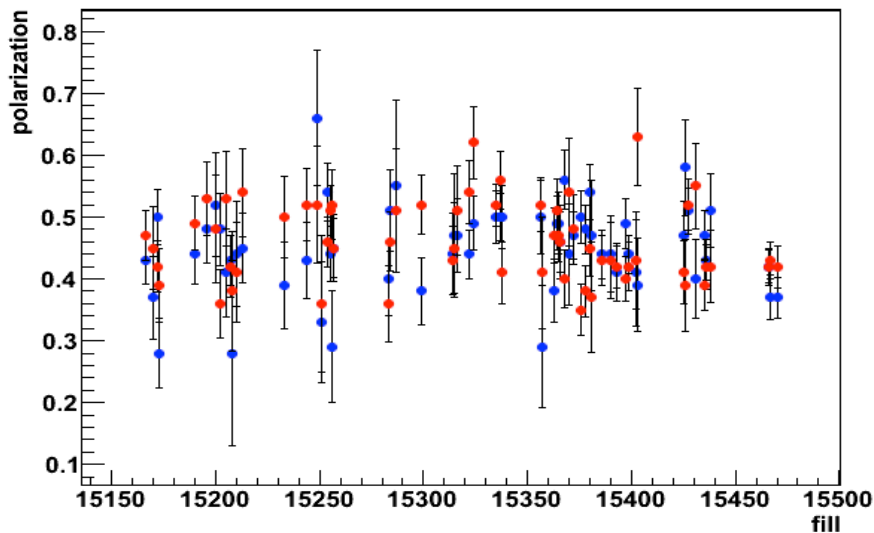


Figure 4.4: Polarizations for the RHIC Yellow and Blue beams, shown as red and blue symbols respectively, as measured with the hydrogen-jet polarimeter during Run 11.

4.4 Request for Run 12

4.4.1 Forward GEM Tracker (FGT) Commissioning and W-physics Measurement

The STAR polarized proton-proton BUR for Run 12 is driven by the commissioning of the Forward GEM Tracker (FGT) and continued collider development at $\sqrt{s} = 500$ GeV, and aims at sampling an integrated luminosity of approximately 190 pb^{-1} with longitudinal beam polarizations of 50% or more in 12 weeks of physics running. This corresponds to an increase over previously sampled data at $\sqrt{s} = 500$ GeV with longitudinal polarizations by more than an order of magnitude. This will extend our measurements of single-spin asymmetries A_L for leptonic W decay to forward and backward electron and positron rapidities, significantly improve the precision of mid-rapidity A_L , and allow for sensitive measurements of A_{LL} in the production of jets and di-jets. The A_L and A_{LL} measurements are sensitive to quark and gluon polarization in the proton, respectively. Following this period, 1 week of polarized proton operations with dedicated beam-optics ($\beta^* = 7$ m) is requested to perform first measurements with the STAR Roman Pots at $\sqrt{s} = 500$ GeV. The latter aim to measure spin asymmetries in elastic scattering and to benchmark the production cross sections for a future glueball search.

The installation of the FGT will occur during the Summer of 2011 along with a new inner support structure. Run 12 will be the first run to take full advantage of the charge-sign discrimination capabilities for forward leptonic W decay electrons and positrons provided by the FGT. Figure 4.5 shows a side view of the new inner tracking system with the planned Heavy Flavor Tracker (HFT) at the center and the FGT on the right side. Also shown is the new East (left side) and the new West (right side) cylindrical mechanical support structure. The W production cross-section in the STAR EEMC acceptance region of $1 < \eta < 2$ is much smaller than at mid rapidity. The W program at RHIC, in particular in the backward / forward rapidity region is a multi-year program.

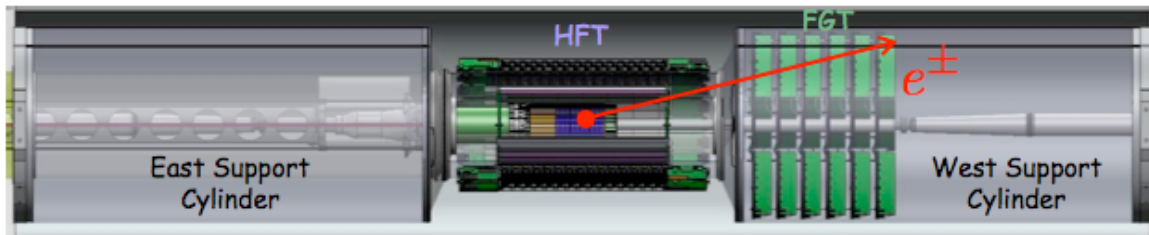


Figure 4.5: Upgrade STAR inner and forward tracking system showing the location of the Heavy Flavor Tracker (HFT) and the Forward GEM Tracker (FGT).

The backward (forward) rapidity region is being accessed depending on which of the polarized proton beams is being considered moving away (towards) the STAR EEMC to

measure the longitudinal single-spin asymmetry for W boson production.

The installation of the FGT will start prior to Run 12 along with a new inner support structure. The design of the FGT quarter sections has been driven by minimizing dead material in general and the dead area region between adjacent quarter sections. This led to the concept of a 2D readout structure realized on a foil rather than on a solid board. In addition, it was attempted to avoid completely a spacer grid between each foil. Maintaining proper HV stability, with this design, turned out to be rather challenging. It was therefore decided to build all quarter sections with a spacer grid. In addition, each quarter section will be mounted onto honeycomb support disks by G10 pins rather than metal pins. This allows to increase the HV stability even further since the HV connecting lines for each GEM foil segment is part of each GEM foil frame.

It turns out that more time is needed to complete this critical element during the full assembly in summer 2011. It is planned to install at least $3 \times 4 = 12$ quarter sections, i.e. 50%. Those quarter sections will be mounted on separate disks thus covering $\frac{3}{4}$ of the nominal coverage in the azimuth angle. It has been shown in the FGT proposal that four quarter sections with a hit resolution of $100\mu\text{m}$ can be used for proper charge sign discrimination. Six disks are required to cover the full vertex region. In order to be able to install as many as possible the FGT quadrants before Run 12 and maximum the vertex coverage for W physics measurement, we therefore request to begin the Run 12 cool-down after January 01, 2012.

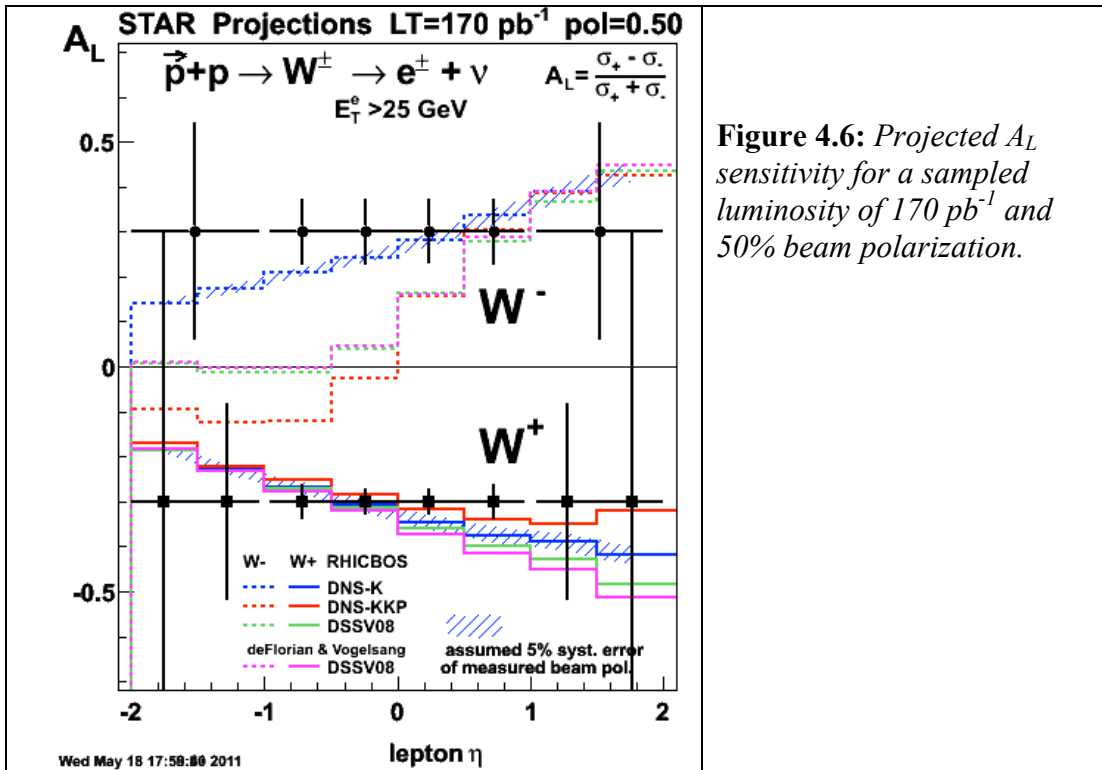


Figure 4.6: Projected A_L sensitivity for a sampled luminosity of 170 pb^{-1} and 50% beam polarization.

The required commissioning of the FGT will make it beneficial to start first with heavy ion running followed by polarized proton-proton running. It is expected that a total commissioning period under beam conditions will require about 3-4 weeks of which 1-2 weeks should be carried out under polarized proton-proton conditions using a high- E_T EEMC trigger requirement. The main commissioning tasks are as follows:

- HV scan of quarter section in addition to cosmic-ray tests
- Commissioning of Front-End Electronics and Data Acquisition System under beam conditions

The longitudinal beam use request for Run 12 aims to significantly improve on the first measurements of the longitudinal single-spin asymmetry A_L for W boson production made in Run 9 [1]. The extension into the backward and forward rapidity region is the main focus of the FGT. The FGT commissioning needs, in particular the high- E_T EEMC trigger requirement, preclude concurrent (low-luminosity) Roman Pot measurements with dedicated beam-optics.

Figure 4.6 shows the projected uncertainty in A_L as a function of the electron/positron rapidity for W boson production with $E_T > 25$ GeV based on an initial data sample corresponding to an integrated luminosity of 170 pb^{-1} and a mean beam polarization of 50%, and forms an intermediate goal of the W physics program. Based on Run-9 experience, we have assumed in our uncertainty estimates that the fraction of background events will be the same as in Run-9 data and that the total W reconstruction efficiency at mid-rapidity will be improved from $\sim 55\%$ to $\sim 65\%$. Measurements of A_L at this intermediate precision will, generally, focus on determining the rapidity dependence over the STAR acceptance region. This will allow to map out different dependencies of A_L on the underlying polarization of quarks and anti-quarks and thus provides meaningful input for a global analysis. Measurements of A_L at mid rapidity will allow a first step in determining the rapidity dependence over four bins as shown in Figure 4.6. It is expected that, at this level of precision, the measurement would start to provide constraining sensitivity to the anti-u quark polarizations for negative lepton rapidities in the case of W^- production. STAR is expected to sample 60% of the delivered luminosity and the full magnitude of RHIC polarization, after tuning of the spin rotator magnet currents.

Figure 4.7 shows the projected performance for a multi-year program based on a recorded data sample of 300 pb^{-1} and a beam polarization of 70%. The projected performance at backward and forward rapidity is based on a rather conservative assumption about the level of signal over background of approximately 1.1. This estimate is based on a full QCD background MC simulation. Assuming that the Run 9 performance of signal over background of approximately 10 at mid rapidity could be also achieved for the backward/forward rapidity region, a reduction of almost a factor two in the achievable uncertainty can be expected. The impact of a large W data sample of similar size as above constraining anti-u and anti-d quark polarizations has recently been shown by a global fit analysis assuming projected data from STAR and PHENIX [6].

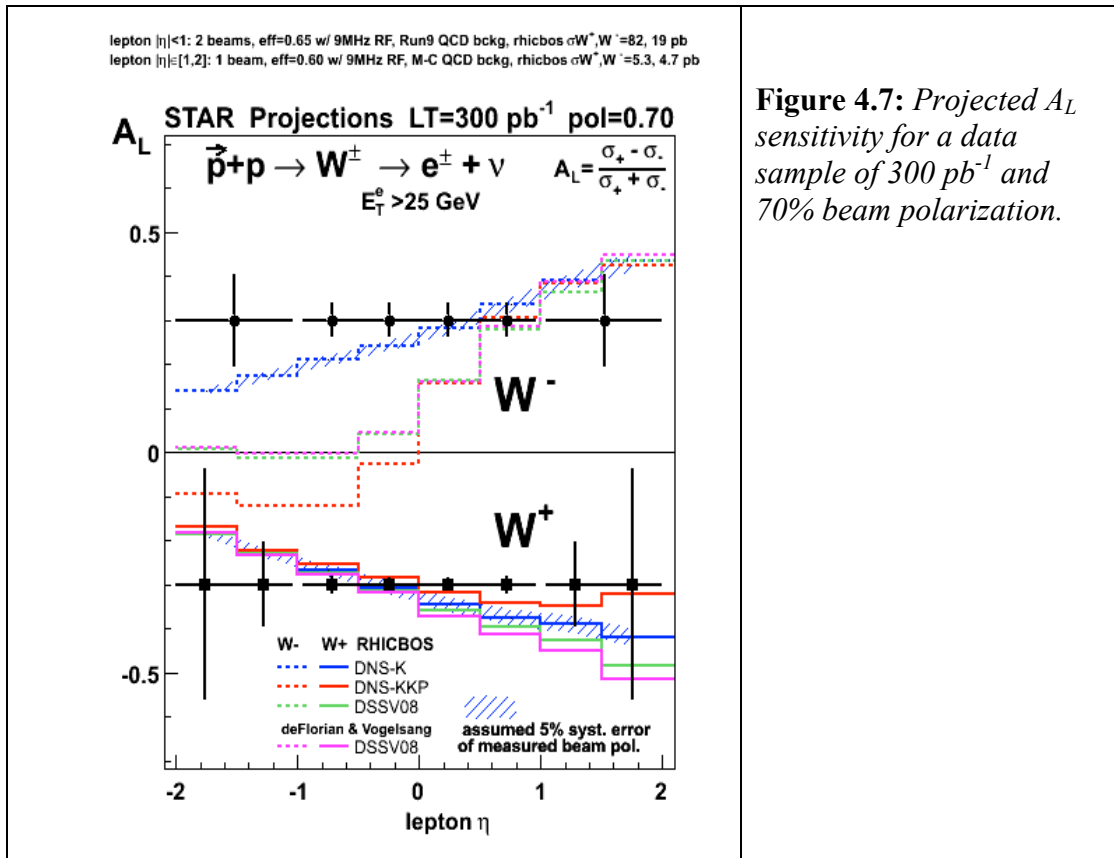


Figure 4.7: Projected A_L sensitivity for a data sample of 300 pb⁻¹ and 70% beam polarization.

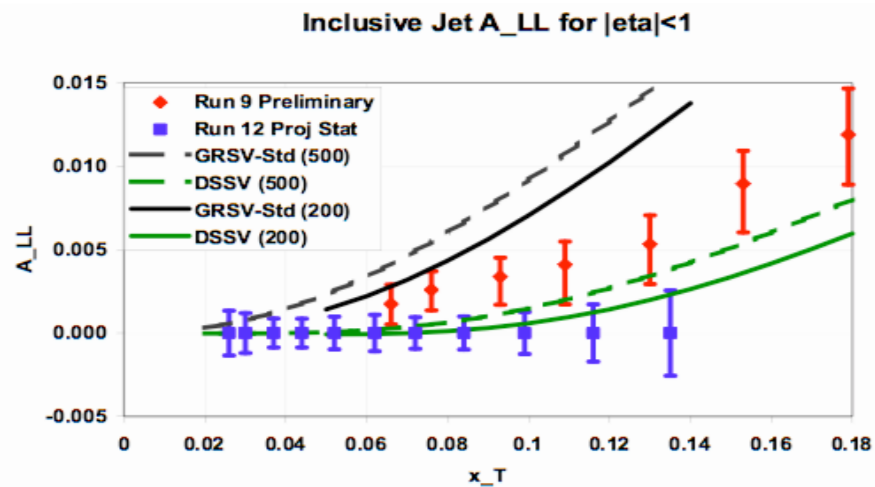


Figure 4.8: A_{LL} projections for inclusive jet measurements at 500 GeV in Run 12 data as function of x_T . The projections are compared with preliminary 200 GeV results from Run 9 and with NLO pQCD evaluations based on two commonly used sets of polarized parton distributions.

Besides the single beam-spin asymmetry measurements of leptonic W-decay, polarized

proton-proton running at $\sqrt{s} = 500$ GeV should allow double beam-spin asymmetry measurements in the production of jets aimed at determining gluon polarization in the polarized proton. For equal pseudo-rapidity and transverse momentum, such measurements are sensitive to smaller gluon fractional momentum fractions (Bjorken- x values) than at $\sqrt{s} = 200$ GeV. The expected values are smaller than at $\sqrt{s} = 200$ GeV. These measurements thus rely crucially on high beam polarizations, comparatively more so than on high luminosity, and adequate control of experiment systematic uncertainties. Figure 4.8 shows the kinematic range and expected statistical uncertainties for inclusive jet A_{LL} measurements at $\sqrt{s} = 500$ GeV versus x_T for a sampled luminosity of 190 pb^{-1} with high- E_T , hence high x_T , triggers. The projections at low x_T are not expected to be limited by integrated luminosity and instead take into account anticipated DAQ hours and known bandwidth limitations. In both cases, beam polarizations of 50% were assumed. The kinematic range and precision of Run 9 preliminary data obtained at $\sqrt{s} = 200$ GeV are shown for comparison, as are NLO pQCD evaluations based on the commonly used GRSV-standard and DSSV sets of polarized parton distributions. In the longer term, using $\sqrt{s} = 500$ GeV data from Run 12 and beyond, we aim to perform also sensitive A_{LL} measurements in the production of di-jets. Figure 4.9 illustrates the anticipated sensitivity for 390 pb^{-1} and 50% polarization (a multi-year goal).

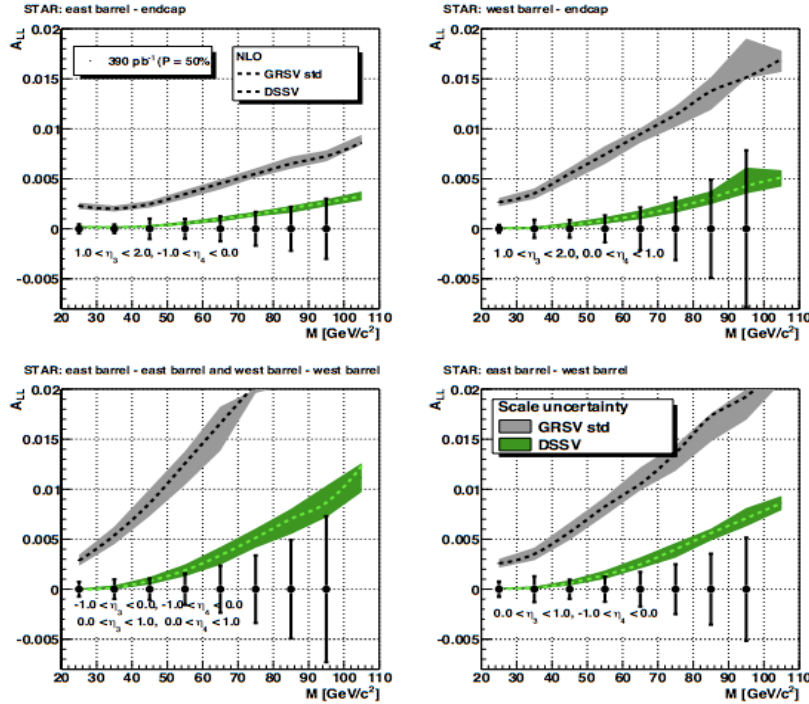


Figure 4.9: Projected A_{LL} for di-jet production for a large, multi-year, 500 GeV data set as function of the di-jet invariant mass M for different pseudo-rapidity regions.

4.4.2 The pp2pp Measurements

In Run 12, we request 1 week of running with dedicated beam-optics settings of $\beta^* = 7.5\text{m}$ and transverse beam polarizations to make spin dependent diffraction measurements with the STAR Roman Pots at $\sqrt{s} = 500\text{ GeV}$. These measurements complement measurements made in Run 9 at $\sqrt{s} = 200\text{ GeV}$ and significantly extend their kinematic range to $-t \sim 0.2\text{ (GeV/c)}^2$. This is illustrated in Figure 4.10, which shows preliminary STAR results from $\sqrt{s} = 200\text{ GeV}$ data obtained in Run 9 and the projected statistical precision versus $-t$ at $\sqrt{s} = 500\text{ GeV}$ for Run 12. The 500 GeV projections are seen to extend the t range of the $\sqrt{s} = 200\text{ GeV}$ data by more than a factor of five with similar precision.

These measurements will thus uniquely complement prior data and help elucidate the \sqrt{s} and t dependence of the single spin analyzing power A_N in elastic scattering. This analyzing power is sensitive to the interference between the one-photon exchange and the strong, hadronic scattering amplitudes in elastic scattering. Their understanding, besides being of fundamental interest, is relevant also to precision polarimetry. The curves in Figure 4.10 show evaluations based on Ref. [10] for the absence of a hadronic spin-flip, signified by the ratio of single-flip to nonflip amplitudes and here denoted by $r_5 = 0$, and extrapolation of the best fit to the data at $\sqrt{s} = 200\text{ GeV}$.

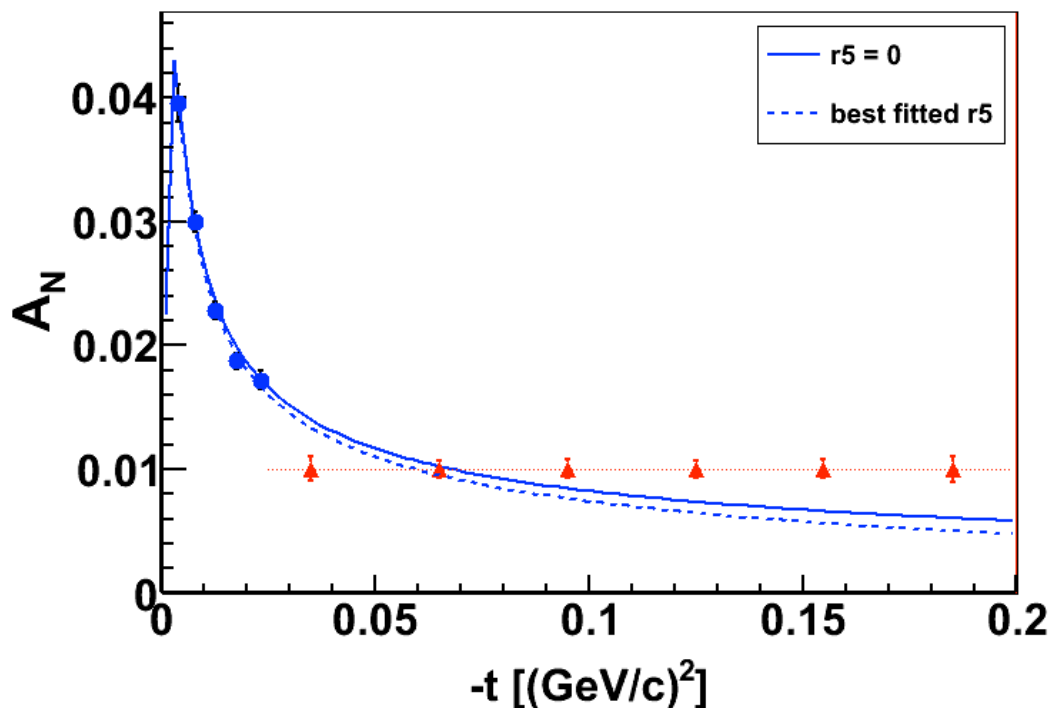


Figure 4.10: Projected statistical precision and kinematic coverage for $\sqrt{s} = 500\text{ GeV}$ measurements (red symbols) of A_N versus t in comparison with preliminary STAR data at $\sqrt{s} = 200\text{ GeV}$ from Run 9 (blue symbols). The curves show model evaluations [10] of A_N for the absence of a spin-flip amplitude ($r_5 = 0$) and based on extrapolation of the best fit to $\sqrt{s} = 200\text{ GeV}$ data.

The requested data at $\sqrt{s} = 500$ GeV should make it possible also to determine the total scattering cross section σ_{TOT} , which has thus far not been measured in proton proton interactions at RHIC energies. Our aim is an uncertainty of about 2%, which will be dominated by the measurement of luminosity, knowledge of beam optics, and other accelerator driven systematics. In addition, the proposed Run 12 measurements will allow us to obtain benchmark yields for coincident central particle production. We anticipate to be able to collect a significant sample of $\sim 50\text{k}$ events in the $\pi^+\pi^+\pi^+$ channel in the proposed one week of running with an estimated luminosity of $10^{30}\text{cm}^{-2}\text{sec}^{-1}$. The benchmarking of these yields is of particular importance to a future glueball search with STAR.

4.5 Scenarios for Run 13

4.5.1 Polarized p+p Collisions

STAR aims to perform several high-priority spin physics measurements beyond Run 12 at $\sqrt{s} = 200$ GeV and at $\sqrt{s} = 500$ GeV. These include, as described in section 4.3, the quark, anti-quark, and gluon polarizations in the polarized proton via high precision measurements of single-spin and double-spin asymmetries of W and jet probes produced at collision energies of $\sqrt{s} = 500$ GeV. The projected RHIC Run 12 performance for $\sqrt{s} = 500$ GeV polarized proton operations show a spread by a factor of 4 or more in integrated luminosity. Run 12 experience at $\sqrt{s} = 500$ GeV is likely to yield much better insights in expected performance for future years. At this time, we consider continued $\sqrt{s} = 500$ GeV running in Run 13 a viable and desirable scenario if a significant physics improvement over the Run 12 data set can be obtained in 8 weeks of beam operation.

STAR also aims to significantly improve its gluon polarization measurements also at $\sqrt{s} = 200$ GeV. Figure 4.1 shows preliminary results on the double-spin asymmetry A_{LL} in inclusive jet production from 20 pb^{-1} sampled in Run 9 at $\sqrt{s} = 200$ GeV with 58% average beam polarization. The data with transverse momenta of ~ 12 GeV/c and higher are statistics (luminosity) limited. The Run 9 data are compared with Run 6 data and with the estimated uncertainty in the NLO pQCD expectation based on the DSSV polarized parton distributions [7]. STAR data from Run 6 form one of the inputs to the DSSV polarized parton distributions, and provide unique sensitivity to the polarized gluon distribution for $0.02 < x < 0.2$. The 3-4 times more precise data from Run 9 have not yet been used in an extraction of the polarized parton distributions, however, their impact is easily assessed by comparison with the DSSV uncertainty band. Further reduction in the uncertainties by a factor of about 2 should be achievable for jet p_{T} larger than 12 GeV/c, based on projected RHIC performance and improvements in STAR sampling efficiency. The uncertainties for jet $p_{\text{T}} = 6\text{--}12$ GeV/c would be reduced by a factor of about $\sqrt{2}$. This would provide significant further constraints on the polarized gluon distribution in the polarized proton, especially for large gluon momentum fractions. Doing so constitutes our second goal for Run 13. Such a data set will also lead to

significant improvement over the recent STAR measurements of di-jet A_{LL} at $\sqrt{s} = 200$ GeV (see Fig. 4.2).

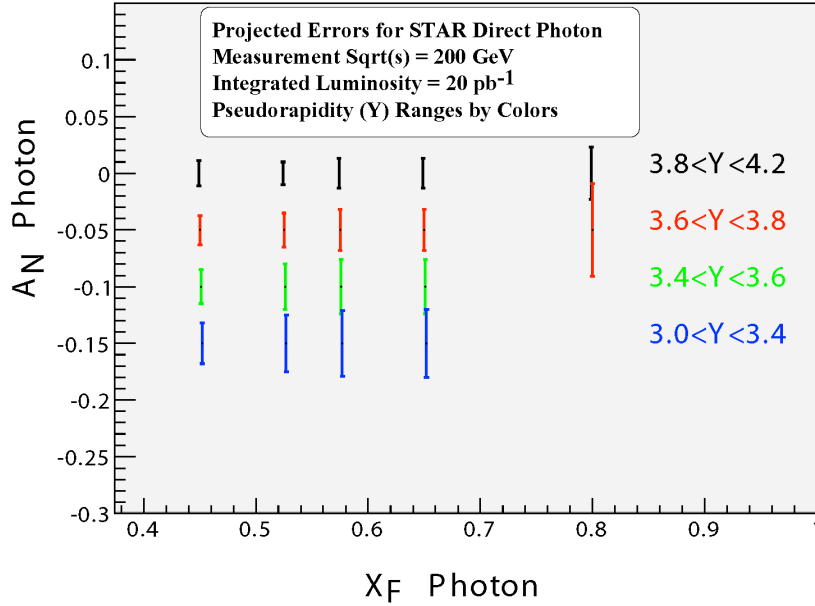


Figure 4.11: Projected uncertainties for a STAR measurement of A_N for direct photon production with an integrated luminosity of 20 pb⁻¹ and 60% polarization.

The third STAR high-priority near-term goal is the measurement of the transverse single spin asymmetry A_N in forward production of prompt photons. The importance of prompt photon A_N has been emphasized in a number of recent publications (see for example [8,9]). STAR has thus far measured sizable asymmetries in the forward region in the production of forward π^0 and η mesons. The production of prompt photons does, in good approximation, not involve fragmentation. The measurement of the transverse single spin asymmetry in their forward production is thus insensitive to the Collins mechanism. The Siverts mechanism has attracted particular attention among the possible explanations for the sizable A_N observed at forward rapidity. Measurement of non-zero prompt photon A_N would provide selective sensitivity to this effect in hadroproduction at hard scales. Its comparison with measurements of the Siverts effect in deep-inelastic polarized lepton-nucleon scattering would be of particular further interest.

Figure 4.11 shows the expected precision for an integrated luminosity of 20 pb⁻¹ with 60% beam polarization. This sensitivity estimate assumes the photon cross section from PYTHIA 6.222, which gives a good description of the forward π^0 cross sections measured by STAR. The primary backgrounds will arise from very asymmetric π^0 and η decays, where only one of the decay photons is observed by the FMS. These background contributions are estimated using our recent measurement of the cross section and transverse single-spin asymmetry for π^0 and η production at $0.4 < x_F < 0.8$ and $\eta=3.68$, using Run 6 FPD data, together with recent experience reconstructing π^0 and η in the Run 9 FMS data that were recorded with 200 GeV p+p collisions. At larger x_F and smaller

rapidity, the backgrounds are predicted to be rather small, and the uncertainties are dominated by the direct photon statistics. In contrast, at smaller x_F and larger rapidity, the backgrounds are expected to be larger. The uncertainties in this region are dominated by the systematics associated with the background subtraction. This means that very good, concurrent measurements of the π^0 and η A_N will also be required. A partial FMS jet patch trigger was implemented before Run 11. The η measurement, in particular, will require that the complete FMS jet patch trigger, including overlapping patches, be implemented before Run 13.

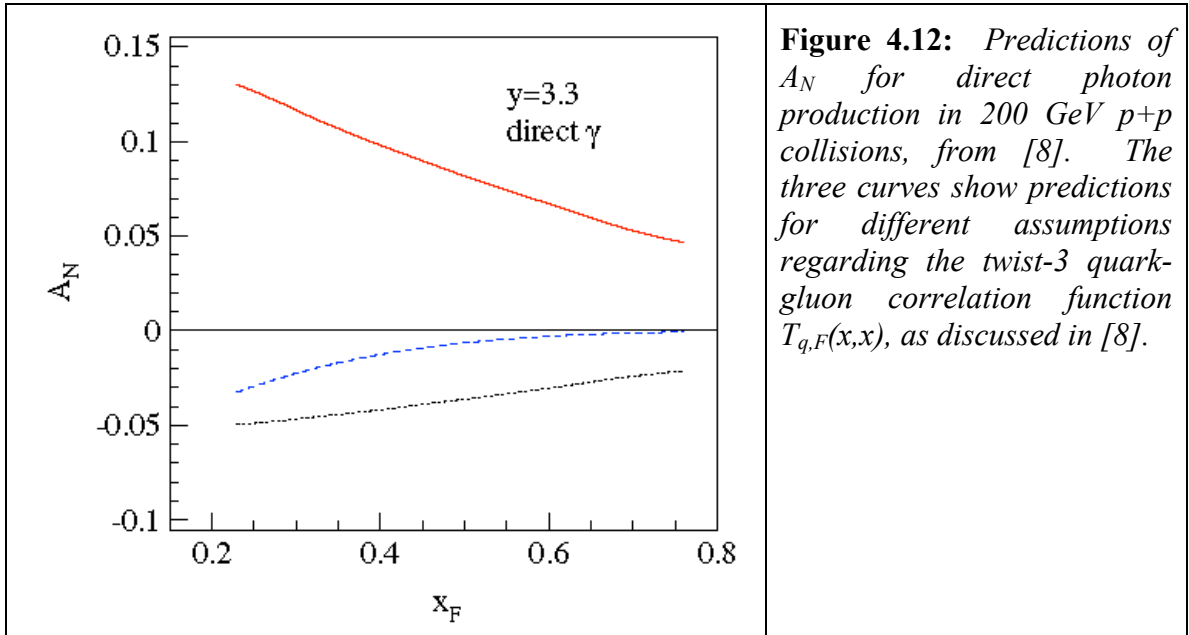


Figure 4.12 shows a recent prediction of A_N for forward direct photon production in 200 GeV $p+p$ collisions. A comparison of Figs. 4.11 and 4.12 demonstrates that STAR will be able to perform a very significant measurement.

The most recent Collider Projection document [2] stated that we could expect luminosities at $\sqrt{s}=200$ GeV to be a factor of two higher in Run 13 than they were during Run 9. A recent communication from W. Fischer [3] confirmed that significantly higher 200 GeV luminosities are still expected in Run 13, though it did not specifically restate the “factor of two”. When combined with improvements in STAR utilization of delivered beam since Run 9 (from $\sim 50\%$ to $\sim 60\%$), this implies STAR should be able to sample an integrated $p+p$ luminosity of 60 pb^{-1} at 200 GeV during a 10-week run.

The beam polarization was close to 60% in both Runs 6 and 9. During Run 11, AGS Jump Quads were commissioned and found to improve the polarization at AGS full energy by close to 10% relative. Additional polarized ion source improvements are anticipated prior to Run 13. Taken together, we consider it reasonable to assume that these improvements will lead to 60% polarization during the beginning of the Run 13 200 GeV period, increasing to an average of 65% by the end of the period. A combination of

20 pb⁻¹ with 60% polarization in transverse mode and 40 pb⁻¹ with 65% polarization in longitudinal mode would suffice to achieve both of the 200 GeV goals described above.

The same sampled luminosity of 60 pb⁻¹ will provide important heavy ion reference data, as discussed in the following section.

References:

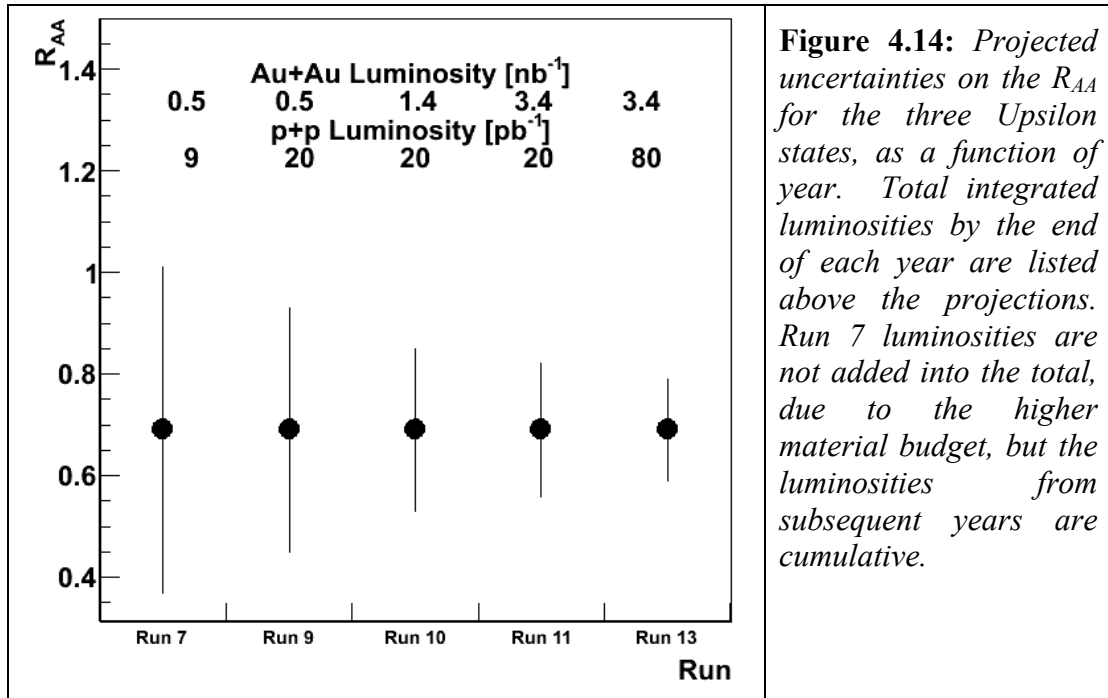
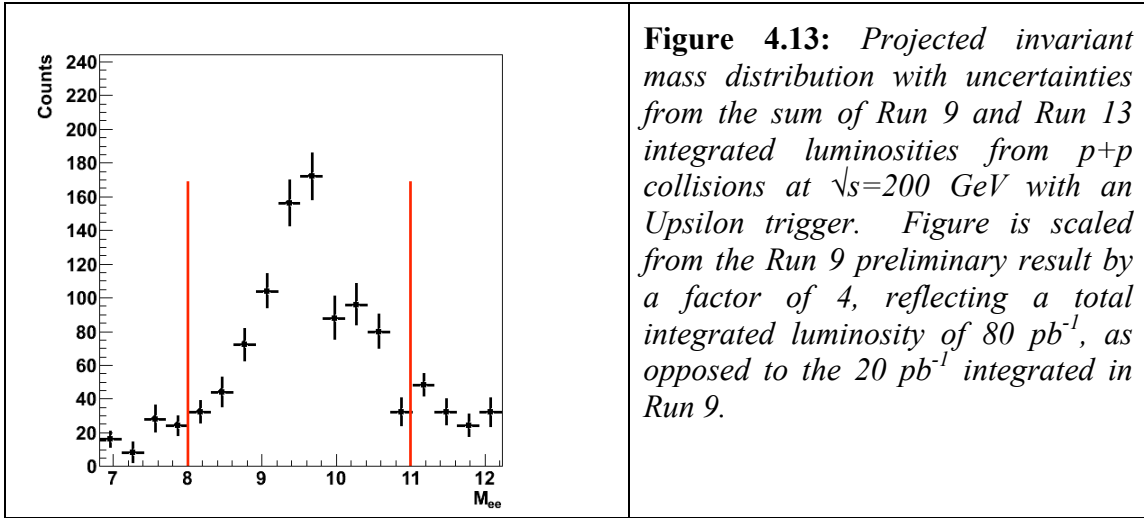
- [1] STAR Coll., M.M. Aggarwal et al, Phys. Rev. Lett. 106: 062002 (2011).
- [2] W. Fischer et al, RHIC Collider Projections (FY2011-FY2015), May 11 2010.
- [3] W. Fischer, private communication 2011.
- [4] P. Djawotho, for the STAR Collaboration, XIX Int. Workshop Deep-Inelastic Scat. Related Subjects (DIS 2011), see https://wiki.bnl.gov/conferences/index.php/Spin_Physics .
- [5] M. Walker, for the STAR Collaboration, XIX Int. Workshop Deep-Inelastic Scat. Related Subjects (DIS 2011), see https://wiki.bnl.gov/conferences/index.php/Spin_Physics .
- [6] D. de Florian and W. Vogelsang, Phys. Rev. D 81: 094020 (2010).
- [7] D. de Florian, R. Sassot, M. Stratmann, and W. Vogelsang Phys. Rev. Lett. 101: 072001 (2008), Phys. Rev. D 80: 034040 (2009).
- [8] Z-B. Kang, J-W. Qiu, W. Vogelsang, and F. Yuan, Phys. Rev. D 83, 094001 (2011).
- [9] K. Kanazawa and Y. Koike, arXiv:1104.0117 (2011).
- [10] T.L. Trueman, Phys. Rev. **D77**:054005, 2008

4.5.2 Heavy ion reference p+p collision in Run 13

Run 13 gives a timely opportunity to return to p+p collisions at $\sqrt{s} = 200$ GeV, in order to obtain reference data for measurements involving electrons. After Run 13, substantial portions of the Heavy Flavor Tracker will be installed, which will introduce additional material, and so increase Bremsstrahlung tails and background from conversions in the electron channel. During Run 13, the Pixel portion of the HFT will be insertable, but can be easily retracted during the p+p running in order to minimize the material budget. Some additional statistical power in Au+Au collisions can be gained during the HFT engineering run, with the Pixel detector inserted, but this will suffer from the additional material budget. In addition, with an expected 50% coverage in the Muon Telescope Detector, comparisons between the electron and muon channel can begin to be made, along with a first look at electron-muon correlations sensitive to the charm contribution to intermediate-mass dileptons.

By Run 13, much of the statistical limitation for luminosity-hungry measurements like the Upsilon in the e⁺ e⁻ channel will be the p+p reference. The p+p integrated luminosity for Upsilon's from Run 9 is 20 pb⁻¹, while the combined Run 10 and Run 11 Au+Au dataset will be ~ 3.4 nb⁻¹, equivalent under binary scaling to 140 pb⁻¹, though with selection on centrality, non-unity R_{AA}, and additional backgrounds in Au+Au the statistical power for equivalent luminosity is somewhat less in Au+Au. An additional 60 pb⁻¹ will bring the statistical uncertainties of the p+p reference on par with that in Au+Au, as projected in Figure 4.13. Figure 4.14 shows the resulting projected uncertainty on the R_{AA} of the sum of the states, as a function of year; with the

combination of Run 11 Au+Au and Run 13 p+p, we expect a statistical uncertainty of 10% on this quantity. In addition, with 50% MTD coverage, we can begin to compare measurements in the muon channel with those in the electron channel.



Another opportunity is in the intermediate and low-mass dielectron channel, which has been enabled by the TOF. First results were obtained in Run 9, with 72% TOF coverage. In Run 13, with 100% TOF coverage and a dataset on the order of 600M minimum bias events, a factor of four higher statistical power is expected, as seen in Figure 4.15. This is crucially important in the intermediate mass region between the ϕ and J/Ψ , where the

current uncertainties are very large, and will also improve the ability to look differentially in p_T across the full invariant mass range. As with the Upsilon, after Run 11 Au+Au data are analyzed, the statistical limitations in this set of measurements will be in the p+p reference.

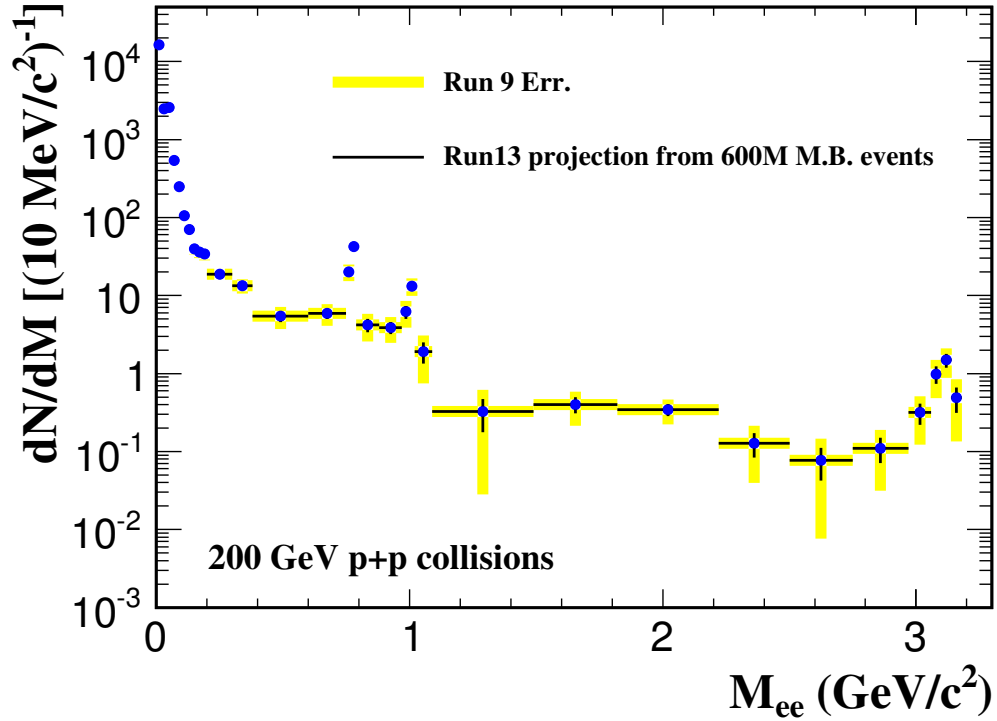


Figure 4.15: Projection of uncertainty on dilepton measurements from Run 13. Yellow bars indicate the current statistical uncertainties from Run 9, while the bars indicate projected uncertainties from Run 13.

5. STAR Heavy Flavor Tracker (HFT) Engineering Run

An engineering run with the HFT PXL detector serves a number of important functions that are required in the development of a robust detector system capable of producing useful physics in a timely fashion. Some functions address resolution of questions that could affect or require modification of the final design. Other functions address the need to get an early start on hardware and software commissioning in order to guarantee physics results from the first run with the HFT.

The engineering run will provide a test for vulnerability to wakefield generated noise or other unanticipated noise sources. We don't expect this to be an issue with our detector design, but if the engineering run exposes a problem then RF shielding would be implemented.

Every effort is being made to insure that the HFT PXL detector will meet the requirements of mechanical stability while operating in the STAR environment. However, if the engineering run reveals difficulties resulting from unanticipated issues with the STAR environment then they can be addressed before operation with the completed HFT detector.

The PXL detector electronics system, detector plus read out, will be tested with the STAR DAQ and trigger system prior to the engineering run so integration complications are not expected, but the engineering run could reveal unexpected issues with pickup or grounding associated with DAQ connections that would require correction prior to the complete HFT operation.

The proposed engineering run will test software for detector alignment through tracking so that good working software is available at the start of operation of the complete HFT detector system. The engineering run will be an important time for commissioning this software as well as other software systems such as slow controls and various diagnostic software tools. There are many such functions that will require testing and correction that can be accomplished only through actual operation. Experience has repeatedly and painfully shown that bringing up a new detector system in a collider environment is a daunting task with many time conflicting activities which are still all essential to proper operation. It is important to recognize this and design an engineering run to provide an ordered approach to commissioning the detector.

Also the full trial assembly sequence of the inner detector support (IDS) with middle support cylinder (MSC), but without the added hassle of also requiring full integration and assembly of the silicon strip detector (SSD) and intermediate silicon tracker (IST) is of great value. There is a lot of structures to come together, and having a trial dry fit of all, together, with the new small beam pipe, a full year before they are fully required to meet physics run requirements, allows us ample time to fix, adjust, or otherwise modify

structures required to support IST, Pixels and the new beam pipe. Pixel insertion in the STAR Hall is no small task. Having the MSC installed, with new beam pipe, in STAR experimental hall, will allow verification of all external installation tooling, and potential interferences, again allows sufficient time for modification before installation ahead of run-14 (Summer/Fall) in 2013.

The limited detector coverage necessary for the engineering run is being configured to provide some capability for D-meson detection so there is possibility that some physics can be accomplished; at minimum confirmation of expected pointing resolution could be verified, demonstration of physics capabilities, but the overriding goal of the engineering run will be system verification and correction.